Online Version

Deliverable D2

Potentials and capabilities of spectroscopic instruments for HCl detection

T. Benoy (PTB)[1], Z. Qu (PTB)[1], O. Werhahn (PTB)[1], V. Ebert (PTB)[1], E A. Curtis (NPL)[2], N. C. G. Black (NPL)[2], G. P. Barwood (NPL)[2], T. Rajamaki (VTT)[3], S. Persijn (VSL)[4], T. Hieta (GASERA)[5]

[1]Physikalisch-Technische Bundesanstalt (PTB), Bundesallee 100, 38116 Braunschweig, Geramany

[2]National Physical Laboratory (NPL), United Kingdom

[3]VTT Technical Research Centre of Finland Ltd, P.O. Box 1000, FI-02044 VTT, Finland

[4]VSL, PO Box 654, 2600 AR Delft, The Netherlands

[5]Gasera Ltd., Lemminkäisenkatu 59, 20520 Turku, Finland

This online version is similar to the version submitted to MSU, except for an updated sequence of sections and for the removal of VTT's contribution due to copyright issue.

DOI: 10.7795/EMPIR.17IND09.RE.20200929

EMPIR Grant Agreement number

17IND09

Project short name

MetAMCII

Deliverable reference number and title

D2 “Report describing the potential and capability of the developed spectroscopic instruments for HCl detection (NICE-OHMS, CRDS, dTDLAS-WMS, miniaturized multipass cell) where the detection target is lower than 1 nmol/mol in less than 1 minute. The report will also cover water insofar as it impacts on HCl Detection (NH_3 was covered in EMRP JRP IND63 MetAMC)”

Organisation name of lead partner for the deliverable

Physikalisch-Technische Bundesanstalt
Braunschweig und Berlin

with partners: NPL, VSL, VTT, GASERA

Due date of the deliverable

30 April 2020

Actual submission date of the deliverable

31 July 2020

This document was drafted based on contributions from: *T. Benoy (PTB), Z. Qu (PTB), O. Werhahn (PTB), V. Ebert (PTB), E A. Curtis (NPL), N. C. G. Black (NPL), G. P. Barwood (NPL), T. Rajamaki (VTT), S. Persijn (VSL), T. Hieta (GASERA)*

Abbreviations

AMC - Airborne molecular contaminants

CRDS - Cavity ring-down spectroscopy

CES - Cavity enhanced spectroscopy

DFB - Distributed feedback (diode laser)

DVB - Devoe Brewer

EOM - Electro-optic modulator

FSR - Free spectral range (of an optical cavity)

FTIR - Fourier transform infrared (spectroscopy)

HITRAN - High-resolution transmission molecular absorption database

NICE-OHMS - Noise-immune cavity-enhanced optical heterodyne molecular spectroscopy

PDH - Pound-Drever-Hall

PAS - Photo-acoustic spectroscopy

dTDLAS - Direct tunable diode laser absorption spectroscopy

WMS - Wavelength modulation spectroscopy

OPO - Optical parametric oscillator

TD-GC-MS - Thermal desorption gas chromatography molecular spectroscopy

ppmv - Parts per million by volume

ppb - Parts per billion by volume

ppt - Parts per trillion by volume

NMI- National metrology institute

OD - Optical depth

CEPAS - cantilever enhanced photoacoustic spectroscopy

QEPAS - quartz enhanced photoacoustic spectroscopy

MOPA - Master oscillator power amplifier

OGS - Optical gas standard

Contents

I. Introduction

The MetAMCII project was established to develop a robust measurement infrastructure for key AMC species such as HCl at those trace concentrations found in cleanroom fabrication environments. This involves development of sensitive and traceable detection methods, low uncertainty static and dynamic reference materials to validate the optical detection techniques, measurement campaigns in cleanroom environments and metrological inter-comparison. Hence, one of the aims of the MetAMCII project is to measure trace levels of key AMC species such as HCl with a target detection of less than 1 nmol/mol in less than a minute which was, so far, difficult to achieve using classical analytical techniques. The focus of the project is on HCl, which is a critical AMC in the semiconductor manufacturing environment. The developed instrumentation should be capable of measuring low levels of AMC molecules with uncertainties ranging from 1% at high concentrations to a few percent at an amount fraction of 1 nmol/mol or less. Unlike other methods such as TD-GC-MS (thermal desorption–gas chromatography-mass spectrometry), spectroscopic systems developed in this project offer advantages of faster detection and relatively low ownership and operational costs at improved chemical selectivity. HCl gas is reactive along the sampling path and corrosive. Hence, sampling of HCl is highly challenging, and calls for coating the wetted parts with inert and hydrophobic surfaces such as SilcoNert® 2000 and Dursan®. Moreover, HCl below the parts per million concentration is unstable for storage in gas cylinders and needs dynamic generation to obtain accurate mixtures at parts-per-billion levels, hence the terminology: dynamic gas standards.

The spectrometers to be developed in the project work on the principle of molecular absorption, wherein the laser is tuned over a selected molecular transition causing attenuation of the transmitted optical signal (an increase in acoustical signal in case of PAS). Due to the small concentration of the gas species, it is often necessary to increase the interaction length of the laser light with the gas molecules using high finesse optical cavities or multipass cells.

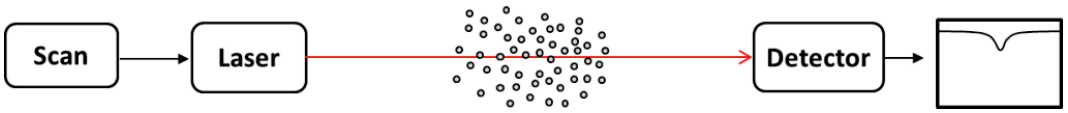

Figure 1 General schematic of laser absorption spectroscopy.

The following optical measurement techniques has been progressed for the MetAMCII project.

(a) Noise-immune cavity-enhanced optical heterodyne molecular spectroscopy (NICE-OHMS)

(b) Mid infrared cavity ringdown spectrometer based on an optical parametric oscillator (OPO-CRDS)

(c) Time division multiplexed direct tunable laser absorption spectroscopy and wavelength modulation spectroscopy (dTDLAS/WMS)

(d) MOPA assisted photoacoustic spectroscopy (MOPA-PAS)

(e) Multi-pass cantilever-enhanced photoacoustic spectroscopy (Multi-CE-PAS)

Table 1 Advantages and disadvantages of each technique and the reported detection limits.

Technique	Pioneering organization	HCl detection limits (in nmol/mol (ppb) and OD $cm^{-1}Hz^{-1/2}$)	Advantages	Disadvantages
NICE-OHMS (Noise-immune, cavity-enhanced, optical heterodyne spectroscopy)	NPL	To be determined through test and calibration with reference standards produced in binary orifice system. Estimated sensitivity in completed device: < 1 nmol/mol in < 1 min.	Transportable, inline detection apparatus. Parts per trillion limits (ppt) can be achieved in NICE-OHMS systems	Complex system, calibration needed, optoelectronic components only available in the in near IR, where absorption lines are weaker
OPO-CRDS	VSL	0.300 nmol/mol, $6{\cdot}10^{-9}$ cm^{-1} $Hz^{-½}$	Mid IR possible, multiple gas species possible. Interaction length of kms	Calibration needed. Expensive to own
dTDLAS/WMS	PTB	~0.380 nmol/mol (@36m, 4.63 10^{-5}), 4.2610^{-8} cm^{-1} $Hz^{-1/2}$	Simpler, faster response times, traceability. "Calibration-free". Typical interaction length of couple of tens of meters. Potential for OGS	Limited by the etalon noise. Only one species possible.
MOPA assisted PAS	VTT	2σ 1.96 ppb with 60s measurement time and 0.40 ppb with 300s measurement time.	Multiple gases possible with the same detector MOPA to enhance sensitivity	Calibration needed. Calibration stability of an emission technique. Stop-flow measurement increases response time
Multi-CE-PAS	Gasera®	~2 ppb in 1 min	Optical transparency, Small volume, Possibility to miniaturize	Matrix dependence. Stop-flow principle

The aim of this report is to summarize the potentials and capabilities of the developed spectroscopic instruments progressed in the project. This involves a description of the individual spectrometers and the detection limits achieved, completed by an uncertainty assessment. The spectrometers which are developed in project will be calibrated/validated using the low-uncertainty dynamic reference gas mixtures developed in a different work package. Since there are no traceable gas standards for HCl at ppm levels and below, these measurements in an intercomparison campaign will help to underpin the NMI certified dynamic gas amount fractions for HCl, necessary to obtain accurate measurements in environments such as semiconductor fabs, or to provide low-uncertainty mixtures to the specialty gas industry.

II. Spectroscopic techniques

1 Time division multiplexed dTDLAS and wavelength modulation spectroscopy - PTB

1.1 Introduction

The spectrometer developed at PTB is based in a principle of time division multiplexed digital wavelength modulation spectroscopy and direct tuneable diode laser absorption spectroscopy. Unlike the other detection techniques which need reference standards for calibration of the instrument, the dTDLAS spectrometer is calibration-free and can provide accurate amount fraction measurements traceable to the SI. The interaction length has been further extended by employing commercially available multipass cells. A TILSAM protocol [1] is followed so that the amount fractions measured using dTDLAS can potentially be traceable to primary reference entities. PTB has coined the term optical gas standard which is able to do calibration-free absolute amount fractions measurements and has the potential to replace primary gas reference standards. The optical gas standard shall be developed using the dTDLAS/WMS methodology. Activity 2.2.4 of this project the involves a comparison campaign between the dynamic gas standard at NPL (using a sonic nozzle dilution device) to the optical gas standard used at PTB.

The detection limit for dTDLAS is typically in the range of 10^{-4} (OD). However, to detect 1 ppb or less HCl within reasonable uncertainty, this noise level is not sufficient for the maximum pathlength of gas cells available (~ 200 m), for a given precision. Hence, a time multiplexed scheme is implemented with an added wavelength modulation signal which can routinely reach detection limits of the order of 10^{-5} or 10^{-6}, and under special conditions could even be extended upto 10^{-7}. The WMS measurements provide improved sensitivity and can be calibrated using dTDLAS.

1.2 Theory

Direct tuneable diode laser spectroscopy (dTDLAS) is the methodology used by PTB to accurately measure the CO_2 amount fraction [2], without using any primary reference mixtures. Like most of the infrared spectroscopy techniques, traditional tuneable direct absorption spectroscopy needs calibration of the measurements with a primary gas standard for traceability.

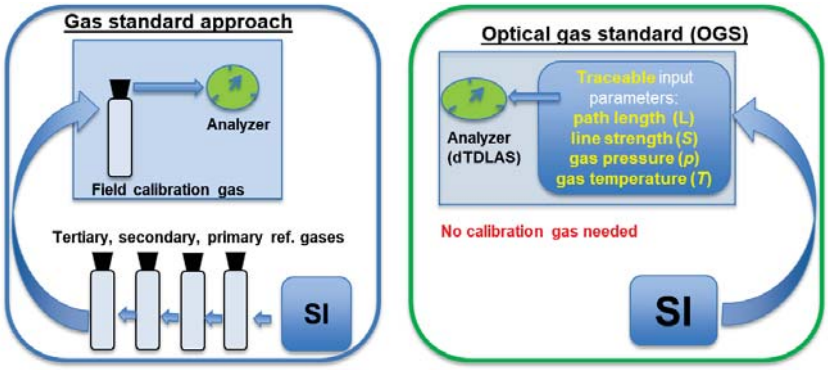

Figure 1.1 Schematic of the gas standard approach and our optical gas standard.

The dTDLAS is implementing the traceable infrared laser-spectrometric amount fraction measurement (TILSAM) method [1][3]. The TILSAM method has the potential as a primary method directly applied, depending on the level of uncertainties that has been estimated for a given system. The method can also be used for field applications. The schematic of the TILSAM is compared with gas standard approach in Fig. 1.

In dTDLAS, the laser is selectively tuned across the selected molecular transition of HCl. The laser light is attenuated at selected wavelengths, through excitation of the vibrational energy levels of the gas molecule. The gas concentration is determined by amount of the light attenuated.

$$I(\lambda) = E(t) + I_0(\lambda)T_r(t)\exp(-S(T)g(\lambda - \lambda_0)nL) \quad (1)$$

E(t) is the background emission of the laser from the spontaneous and side mode emissions, I_0 is the incident laser light energy, $T_r(t)$ is non-absorption related transmission losses, *S(T)* is the line strength at gas temperature *T*, $g(\lambda - \lambda_0)$ is the molecular absorption line shape function, *n* is the number density, and *L* is the effective optical pathlength.

The gas concentration is determined using the area under the absorption line using a Voight fit, which is a convolution of the Lorentzian and doppler broadened profiles keeping the doppler broadening width (for a fixed temperature) as a constant.

$$x = \frac{k_B T A_{line}}{p_{total} S(T) r_{iso} L} \quad (2)$$

where k_B is the Boltzmann constant, *T* is the gas temperature, p_{total} is the total gas pressure, A_{line} is the measured line area, and r_{iso} an isotopic correction factor matching the line strength *S(T)* taken from references to the isotopic abundances in the gas that is actually measured.

The line strength at temperature *T* is given using the equation:

$$S(T) = S_0 \left(\frac{Q_{To}}{Q_T}\right) * exp\left(-h * c * \frac{E}{k_B} * \left(\frac{1}{T} - \frac{1}{T_0}\right)\right) \quad (3)$$

S_0 is the line strength at a reference temperature T_0 (296 K) and *Q* is the total internal partition function, *h* is the Planks constant and *c* is the speed of light in vacuum.

The amount fraction *x* measured by dTDLAS is traceable to the SI, if the influence quantities given in equation (1) are traceable to the SI.

Wavelength modulation spectroscopy involves applying an additional current dither to the laser diode and demodulation the signal away from the *1/f* noise band enabling a lower noise floor for the measurements [4][5].

The laser current is modulated by applying a current dither to the laser diode, apart from the linear scan.

The intensity output of the laser is given as,

$$I_l(\nu) = I(\nu)\{1 + i_0(\nu)\cos(\omega t + \psi_1) + i_2(\nu)\cos(2\omega t + \psi_2)\} \quad (4)$$

where,

$$i_0 = \frac{\Delta I(\nu)}{I(\nu)}, i_2 = \frac{\Delta I_2(\nu)}{I(\nu)} \quad (5)$$

are constants for a given DFB laser [4], ω is the frequency of the sinusoidal modulation, $I(\nu)$ is the instantaneous intensity of laser, $\Delta I(\nu)$ and $\Delta I_2(\nu)$ are the amplitudes of linear and nonlinear intensity modulations respectively, ψ_1 is the phase of the frequency modulation (FM) relative to intensity modulation (IM) and ψ_2 is the phase of the nonlinear IM relative to the linear FM.

The current modulation also leads to modulation of the laser output frequency via the fast carrier and slow thermal effects as follows,

$$\nu = \nu_1 + \Delta\nu\cos(\omega t) \quad (6)$$

where ν_1 is the instantaneous frequency of the laser, $\Delta\nu$ is the frequency modulation amplitude. The modulation index (m) is an important entity in WMS defined as the ratio of the laser frequency modulation amplitude to the half with at half maximum of the selected absorption feature. The modulation amplitude is a function of the dynamic tuning coefficient of the laser [6] and measured using wavelength selective elements such as etalons or fibre ring resonators. The first harmonic signal peaks at m= 1 and the second harmonic signal peaks at m= 2.2.

The detector signal is demodulated using a lock in amplifier at the various harmonics. For an optically thick sample, assuming the *2f* signal is aligned with the X-channel of the lock in amplifier (LIA); the *2f* signals on the *X* and *Y* channels of the lock-in amplifier are derived as follows [6]:

$$X_{2f} = \frac{GI}{2}\left[H_2 + \frac{i_0}{2}(H_1 + H_3)\cos(\psi_1) + i_2\left(H_0 + \frac{H_4}{2}\right)\cos(\psi_2)\right] \quad (8)$$

$$Y_{2f} = -\frac{GI}{2}\left[\frac{i_0}{2}(H_1 - H_3)\sin(\psi_1) + i_2\left(H_0 - \frac{H_4}{2}\right)\sin(\psi_2)\right] \quad (9)$$

where the constant G accounts for the channel gain for the LIA. The maximum signal is obtained on the lock-in phase of the signal. H represents the Fourier expansion coefficients of the gas absorption line. IT has a first derivative line shape for 1f, the characteristic derivative shape for 2f and so forth. The above equation states the second harmonic demodulation, the signal is dominated by a signal with a second derivative line shape.

Similarly, for *1f* demodulation, the major signal components are given as:

$$X_{1f} = \frac{GI}{2}[H_1 + i_0(H_0 + 0.5\,H)\cos\psi_1 + i_2(H_1 + H_3)\cos\psi_2] \quad (10)$$

$$Y_{1f} = -\frac{GI}{2}[i_0(H - 0.5\,H_2)\,sin\,\psi_1 + i_2(H_1 - H_3)\sin\psi_1] \quad (11)$$

It is often customary to represent the resultant of the two signals as

$$R_{1f} = \sqrt{X_{1f}^2 + Y_{1f}^2} \tag{12}$$

Similarly, the background *2f* signals can be given as:

$$X_{2f}^{bk} = \frac{1}{2} GIi_2 \cos\psi_1 \tag{13}$$

$$Y_{2f}^{bk} = -\frac{1}{2} GIi_2 \sin\psi_1 \tag{14}$$

And for and the resultant background signals are given as,

$$R_{2f}^{bk} = \frac{1}{2} GIi_2 \tag{15}$$

$$R_{1f}^{bk} = \frac{1}{2} GIi_0 \tag{16}$$

Ii_1 and Ii_2 being ΔI_1 and ΔI_2, which shows the background originates from the linear and nonlinear intensity modulation, respectively. The background intensity modulation signals are also called the residual amplitude modulation (RAM) signals.

It has been reported by Ebert et al.[7] that the first harmonic signal can be used to cancel the effects of the laser intensity fluctuations. Furthermore, the intensity variations can be cancelled, and background RAM signals subtracted using the formulation:

$$WMS\ signal = \frac{(X_{2f} - X_{2f}^{bk})}{mean(R_{1f}^{bk})} \tag{17}$$

A correlation based scheme is used to calibrate the WMS measurements using dTDLAS [8], which utilizes the information on the entire absorption feature, rather than peak centroid. Additionally, a wavelength drift compensation has been implemented to correct for drifts in the centre wavelength of the laser, between the reference and the calibrated signals. A methodology similar to Rieker et al. [6] is also tested and validated.

1.3 Line selection and measurement conditions

The spectral absorption band of HCl in the wavelength from 1 to 5 microns is shown in figure 1.2. Due to the linear nature of the HCl molecule, its IR rovibrational lines are fewer and well-spaced. In this work we have chosen the strong fundamental band of HCl near 3.6 µm. The measurement gas matrix and measurement conditions was used to choose the optimal gas absorption line for the application.

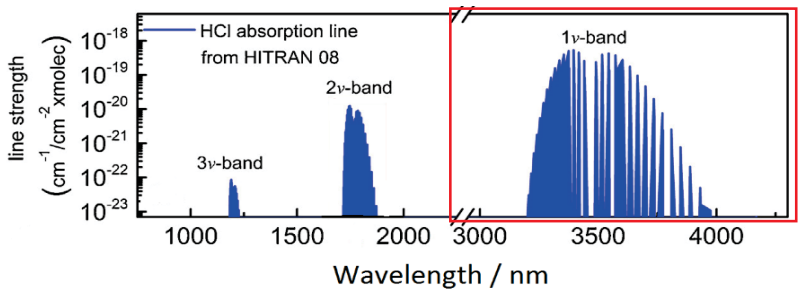

Figure 1.2 The infrared absorption fingerprint of HCl gas molecule.

The choice of the gas line for a given dTDLAS application is governed by several factors; namely its chemical selectivity, peak OD (SNR) and temperature sensitivity. The measurement matrix simulation was done using the major gases which are known to have absorbance in the fundamental band of HCl. The concentrations of the possible interfering species were estimated from a literature survey of indoor air and is shown in table below:

Table 1.1 Species which have interferences with the fundamental band of HCl gas molecule and anticipated concentration levels of the gases in a cleanroom fab.

H_2O	5×10^{-3}	5000 µmol/mol (<8000 µmol/mol in cleanroom fabs)
CO_2	400×10^{-6}	400 to 1000 µmol/mol (Indoor air quality)
CH_4	$5e\times10^{-6}$	2 to 5 µmol/mol (Indoor air quality)
H_2CO	8×10^{-9}	8 to 100 nmol/mol (Indoor air quality) [9]

Chemical selectivity defines how well the gas line is isolated from interfering species inside and outside the measurement volume. We have devised a new metric for the chemical selectivity, namely, the figure of merit (FOM) defined as the peak absorbance (OD) divided by the peak absorbance (OD) of the residuals (gas + matrix spectra). An alternate metric for chemical selectivity is the peak normalised residuals, which is the peak OD of the gas line divided by the sum of the residuals over two times the linewidth of the gas line. A simple line selection algorithm [10], was implemented using the HITRAN 2018 database for fundamental absorption region of the gas molecule at the target concentration of 1 nmol/mol. The temperature range in the cleanroom was set at an average temperature of 20 °C, fluctuating by +-5 degrees assuming worse case. The potential lines suitable for HCl measurements were computed as shown below. From the results it was concluded that the P5 gas line showed the optimal results in terms of peak absorbance and chemical selectivity, and hence was chosen as the targeted gas line for this work. The temperature fluctuations were estimated of the order of 0.1°C, from previous experience and only accounts for an error factor of 0.01 %. The gas pressure fluctuations were assumed to be negligible for the work. This is a very useful approach for line selection.

Table 1.2 Potential lines in the fundamental band of HCl. Assumed pathlength = 36 m, pressure = 100 mbar, amount fraction = 1 nmol/mol, temperature = 20 °C.

no	Line	Wavelength (nm)	Peak absorbance	Peak normalized residuals	Temperature stability (%/K(for S(T))
1	P5	3602.6	1.30×10^{-3}	0.0036	0.1565
2	P6	3633	1.10×10^{-3}	0.01798	0.0532
3	R5	3333.5	1.43×10^{-3}	0.01713	0.1565
4		3699.6	4.40×10^{-4}	0.0056	0.5736
5		3666	7.00×10^{-4}	0.0073	0.2959
6	P 2	3516.6	1.15×10^{-3}	0.013	0.5756

Choice of the gas pressure and cell length

The choice of the gas absorption line from HITRAN survey is described in the previous section. Further, it is necessary to choose the optimal gas pressure and pathlength. It was observed that the optimal chemical selectivity was observed at a pressure of 100 mbar and less. While for some lines, a marked improvement was noted, for other species, this was not the case as for the P5 line. This was due to direct overlap with a formaldehyde line as shown in Figure 1.3. Measurements below 100 mbar are not desirable due to the drop in the signal amplitude. For a 1 ppb detection limit, the available gas cells at 30 m, 36 m and 76 m were used. The choice of the gas cell is also governed by the cell volume in case of reactive gases such as HCl. Figure 1.3 and table 1.2 summarizes the selected gas absorption line plotted with possible interfering species in its spectra window. It is important to note that such careful planning is necessary for selection of the gas absorption line for a given high-resolution spectroscopy application.

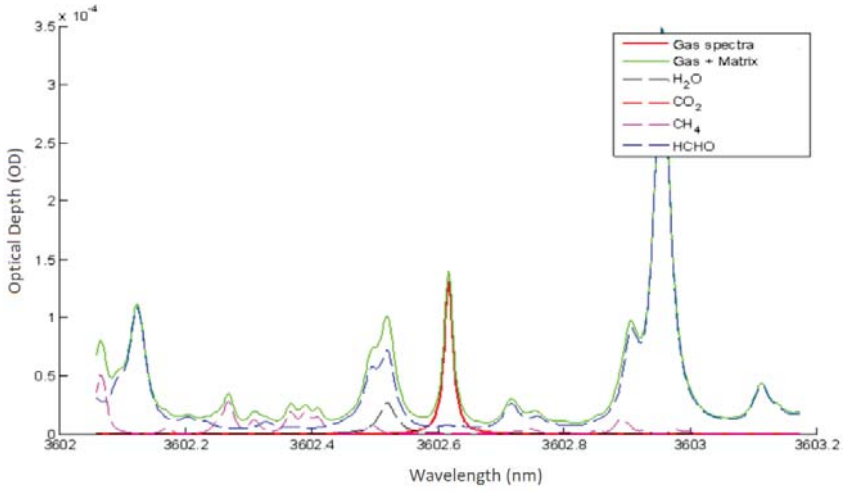

Figure 1.3: From simulation, the best line for the current application is identified as the HCl P5. The simulation above is at 100 mbar, with the cell pathlength of 36 m and a concentration of 1 ppb for HCl for the P5 line corresponding do the application scenario of MetAMCII. The matrix gas composition was adopted from industrial standards indicated in Table 1.1.

Table 1.3 Spectral parameters for the chosen gas absorption line. The line-strength uncertainty is 1-2%.

Gas/laser	Line center (nm/cm^{-1})	Strength (cm/mol)	Self-broadening coefficient (cm^{-1}/atm)	Air broadening coefficient (cm^{-1}/atm)	Temperature dependence exponent (n)	Pressure induced line shift (cm^{-1})	E''
HCl (P5)	3602 /2775.7605	2.886×10^{-19}	0.0223	0.0541	0.223	0.46	312.73110
Uncertainty (HITRAN)	10-20%	1-2%	2-5%	1-2%	5-10%	10-20%	-0.007700

1.4 Instrumentation

Figure 1.4 shows the schematic of the time division multiplexed dTDALS/WMS OGS spectrometer. An arbitrary function generator (Arbstudio 1104) is used to produce alternate time-multiplexed triangular signals (125 Hz), with one of the signals having an additional 20 kHz sinusiodal dither superimposed on it for phase sensitive detection (WMS). The voltage signal is fed into a current controller (Thorlabs LDC 8002, BW@ 200 kHz). The laser temperature is controlled using a Peltier controller (TED 2000). The LDC and temperature controllers are placed on a modular chassis (Thorlabs Pro 8000). The laser source used is a 3.6 um interband cascade laser temperature tuned to the HCl P5 line (reference cell used) and the detector used is an MCT based detector (Vigo). Several multipass cells were used at different stages of the project. The temperature sensor used is the PT100 and the pressure sensor is MKS 640. The length of the multipass cell is measured in a separate experiment, using a Bosch 610 laser distance meter calibrated against a PTB length standard. The signal is subsequently split into two channels and fed to an NI PXI oscilloscope (NI 5122, sampling rate =10 MS/s). One of the channels has a the high pass filter amplifier (SR 640) and is used to implement a digital lock in (Fc = 4 kHz) scheme outlined in previous works[7][8][11]. The other channel is down- sampled by block averaging 40 points to remove the excess noise from the initial signal sampled at a rate of 10 MS/s and is used for dTDLAS. The higher sampling rate of 10MS/s on channel-2 of the ADC is needed for wavelength modulation spectroscopy.

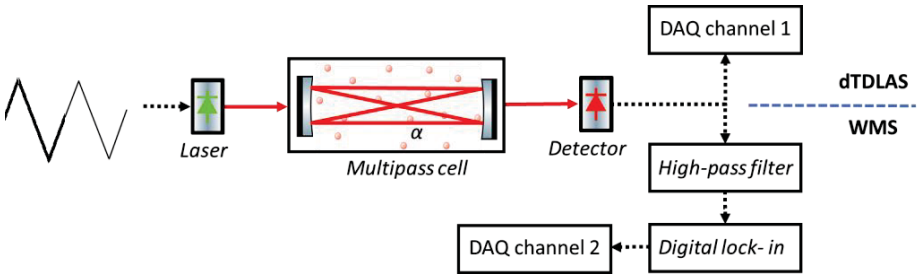

Figure 1.4 Schematic diagram of time multiplexed dTDLAS/WMS spectrometer developed at PTB.

The signal is optimized using recommendations provided in a previous work [11]. The noise floor (LoD) ultimately limited by the ADC noise.

The upper safety exposure limit of HCl is approximately 2 µmol/mol (TRGS 900), hence HCl measurements had to take place in a fume hood, and the HCl gas cylinder be placed in special cabinets. Gaseous HCl is

difficult to sample due to reasons of toxicity and chemical interaction to the substrate. When selecting the tubing, porosity, corrosion and adsorption are the defining factors [12]. 316 stainless steel is the preferred substrate for corrosive gases like HCl [12]. It is well known that amorphous silicon coatings are inert, hydrophobic and corrosion resistant), and are superior to other passivation techniques [13]. Inertness is defined as a state of absence of interactions. Several silicon-based coatings are available such as SilcoNert® 2000, which are CVD deposited onto the surface of the steel at elevated temperatures (300 to 500 °C)[14]. There are few articles that gives a good comparison between SilcoNert® 2000 (Sulfinert®) and Dursan®. SilcoNert® 2000 is the most inert coating and used for process control applications. However, Dursan® has slightly better hydrophobic characteristics and offer similar inertness, therefore, offers a longer shelf life in case moisture is present[15]. Therefore, Dursan® has been chosen for the current application as an "all-rounder" coating. These coatings though effective in reducing the system response times and surface inertness to the measurement process, also significantly increase the cost of the sampling system. For example, coating of the ball valve would cost twice as much as the valve itself (550€), as the valve has to be disassembled before CVD coating and reassembled. It is however critical to observe that majority of the interaction surface area (~98%), is inside the gas cell, which is not coated. Sampling components downstream the cell is not coated as they don't influence the analyte. The gas manifold is prepared to include the dynamic dilution device and 1/10 ppm gas mixture to be transported to PTB. One of the downsides of HCl gas is higher costs involved in replacement of damaged equipment in long term use and the associated times needed to replace damaged parts especially for the mirrors which were reported even for lower concentrations. Hence, the spectrometer is initially tested with a surrogate gas which later involves merely a change in the laser and detector when testing with HCl.

Bypass calibration

A bypass calibration system was implemented for the dTDLAS/WMS spectrometer. Bypass calibration refers to a scenario in which the WMS measurements are calibrated at a generated higher amount fraction by the dTDLAS-measured amount fractions to it, within the linear calibration regime. Five known concentrations will be generated using a dilution device in case multi-point calibration scheme is desirable as shown below, diluting from a high concentration gas mixture. The region of calibration is described in previous works, typically, it could be taken as the region where the dTDAS signal to noise is sufficient (typically > 30). The bypass calibration scheme is advantageous as a gas standard is not needed for sensitive traceable WMS measurements on the dynamic gas mixtures.

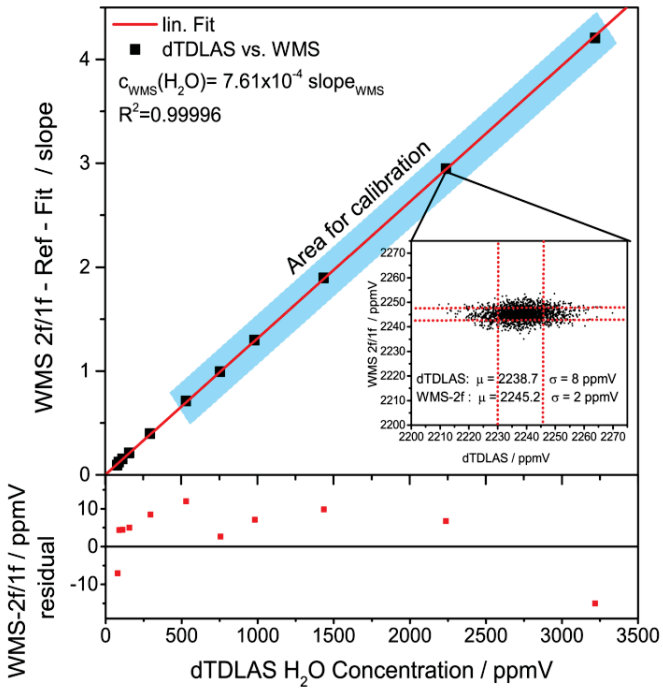

Figure 1.5 Region of calibration and uncertainty assessment. Figure 1.5 is from a previous work at PTB [8].

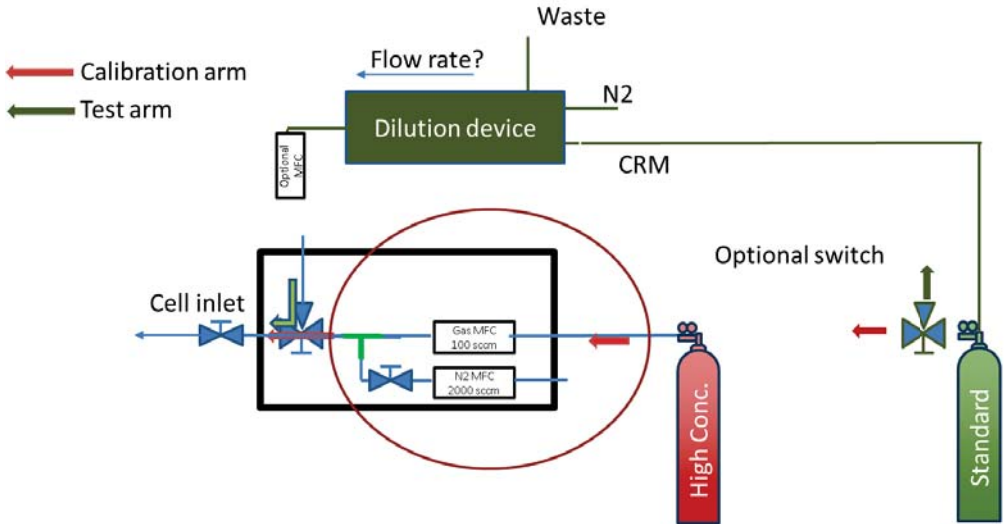

Figure 1.6
Bypass calibration manifold build at PTB for testing of NPLs dynamic gas standard. The high concentration gas bottle diluted amount fractions are used to generate the dTDLAS OGS measurements which can be used to "calibrate" the WMS measurements. Optical gas standards are especially gaining importance in case of hard-to-sample gas species such as HCl.

Optical gas cells

Three gas cells have been tested in this work namely a 36 m astigmatic multipass cell (Aerodyne AMAC 36) and two Herriott gas cells (10.45 m and 30 m, Thorlabs), the former having a Lissajous type of beam spot pattern on the end mirrors and the latter having a circular beam spot pattern. The noise floor of the gas cells is initially tested. The gas cells have been leak tested at low and high pressures to meet manufacturer specifications. The fringe levels are monitored. Using wedged windows is seen to reduce the effect of low FSR fringes which are problematic when implementing baseline fitting. The CaF_2 windows are replaced with of BaF_2 for increased transmission. Nevertheless, it is observed that the noise floor is affected by the high FSR fringes caused by the long pathlength of the gas cells. Figure 1.9 shows the robust optical alignment procedure used for the three multipass cells used in this work. The length of the gas cells is calibrated using a traceable distance meter to have very low standard uncertainties (~0.05%).

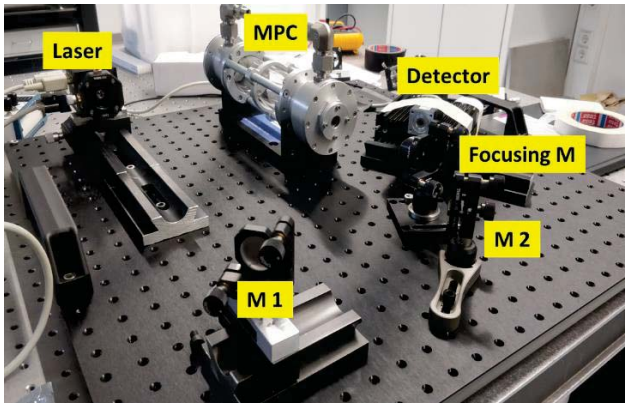

Figure 1.7 The spectrometer is designed to be readily transportable to the fume hood for HCl measurements, or field tests on 19" racks. The optical layout is common for all the gas cells used.

1.5 Initial results obtained using surrogate gas testing

Initial testing using a surrogate gas prevents long term exposure of the expensive gas cells to the corrosive gas and is an alternative when using toxic or corrosive gases. CO_2 has been used as the surrogate gas for this work. Figure 1.9 shows the measured WMS signals for surrogate gas CO_2. A laser plug and play setup is designed using a pinhole arrangement, where the 3.6 um ICL laser can replace the surrogate gas laser without change of the gas sampling line and HCl tests can be readily carried out with only a change of the line-strength keeping the electrical and optical system intact.

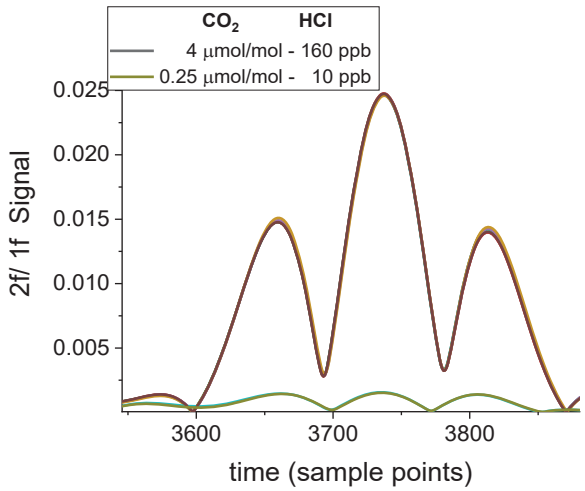

Figure 1.9 Corresponding signals using the formulation by Rieker et al.[6] 10 consecutive signals (100 pre averages) are plotted for each concentration to show the repeatability of the measurements. The digital lock in scheme gives the freedom to test different WMS approaches in a modular developmental platform.

1.6 Performance parameters from the calibration curve

Figure 1.10 shows the calibration curve for the measurement.

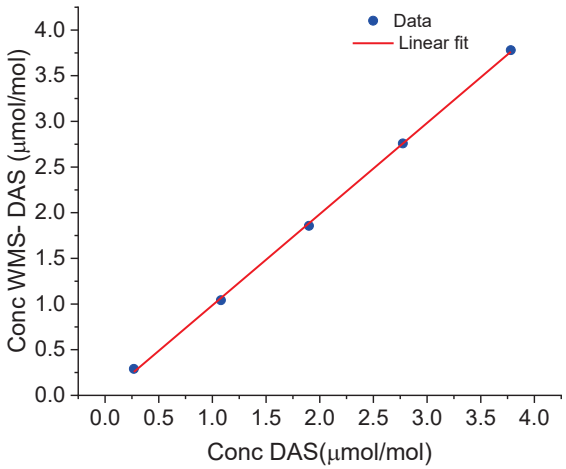

Figure 1.10 WMS signal and calibration curve for a reference concentration of ~4 µmol/mol equivalent of HCl. The intercept represents a bias. x-axis shows scan time in sample points.

Apart from the methods used in previous section, EURACHEM gives the following guidelines for estimating the LoD; (a) using the calibration plot and (b) using the blank or zero analyte measurements. These methods are also briefly outlined in the deliverable D7 (Specifications for laboratory and field tests). When describing analytical sensors, it is also customary to define the limit of quantification. The limit of quantification (LoQ) is defined as the lowest analyte concentration that can be quantitatively detected with a stated accuracy and precision. Two methods of determination of the LoD and LoQ values are found in literature and described below.

LoD and LOQ from the regression curve

The EURACHEM gives a good guideline for the measurement of the limit of detection and uncertainty (treated in the next section). The limit of detection and quantification are defined using the following formulae:

$$LoD = 3.3 * SD / m \quad (18)$$

$$LoQ = 10 * SD / m \quad (19)$$

where SD is deduced from the standard error of the y intercept or the standard deviation of calibration residuals, and m is the slope of the regression analysis. From figure 13, the slope intercept error (= 0.025 µmol/mol) and SD of regression residual (= 0.026 µmol/mol) give similar values.

Using the above equations, limit of detection is calculated as = 3.3 x 0.025 (µmol/mol)/0.9806 = 82 nmol/mol (for CO_2) which is equivalent to 4 nmol/mol of HCl gas.

The quantifiable concentration estimated using the LoQ is given estimated as 254 nmol/mol for CO2 which is equivalent to 12 nmol/mol for HCl.

1.7 Uncertainty estimation methodology for dTDLAS/WMS

The Guide To Estimation of Uncertainty in Measurement (the GUM) [16], gives recommendations for estimating the standard uncertainty. A detailed methodology for estimating the uncertainty of dTDLAS measurements be found in our previous works [17][18]. The line area is measured as described before and equation (2) is used for the analysis of uncertainty (GUM workbench). The pressure and temperature are measured using PTB calibrated sensors accounting for possible drifts during the spectrometer testing period, typically calibrated every year. As it is a well isolated line, it observed that majority of the contribution to the total uncertainty originates from the of the frequency axis, contributed by the uncertainty in free spectral range, and from the molecular line strength. PTB is running a parallel project to improve the frequency scale accuracy, the major contributing factor being the free spectral range [2], using an air spaced etalon and a high accuracy wave meter. Apart from this the pathlength of the multi-pass cell is obtained using a traceable distance meter as discussed previously.

For the dTDLAS calibrated WMS measurements the resultant uncertainty for a single point calibration methodology discussed in previous works [8], for single shot non averaged measurements is written as:

$$u(x) = \sqrt{\frac{S_{WMS}^2}{\sqrt{n}} + u_{dTDLAS}^2 + SD_{resid}{}^2} \quad (22)$$

where S_{WMS} is the standard deviation of the single shot WMS measurements, n is the number of WMS measurements, u_{dTDLAS} is the uncertainty of the dTDLAS measured amount fraction of the primary calibration point and SD_{resid} is the standard deviation of the correlation-fit residuals.

1.8 Measurements and standard tests

The following standard tests and measurements will be completed using HCl gas.

(A) Validation of dynamic gas standards with dTDLAS/WMS optical gas standard

The optical gas standard is implemented through the dTDLAS /WMS scheme. One of the aims of the project is to compare the dTDLAS/WMS optical standard for HCl to the dynamic gaseous standards generated using the critical orifice device of NPL. A dynamic dilution device (two stage critical orifice) and a 10-ppm parent gas mixture, with a combined total uncertainty of less than 0.5% is to be transported to PTB for this. It is recommended to use at least five equally spaced calibration mixtures for linear calibration and the intercomparison. PTB will also qualify the spectral parameters for HCl from these measurements.

(B) ***Evaluation of the bypass calibration scheme***

Determination of the calibration interval of a spectrometer is critical to maintain the required accuracy, as the measurements drift over time. This interval is determined by estimating the drift in the WMS based concentration measurements over different time scales. Though the WMS technique is intensity independent, the long-term drift needs to be investigated. The long-term variation should depend of the laser and the detector, as well as apparent drift of the optical fringes.

(C) Standard tests and uncertainty estimation

The standard performance evaluation tests using the spectrometer are outlined in the "Specifications for laboratory and field tests" document [19], such as zero drift, span drift, response and recovery times, and measurement uncertainty over the entire concentration range. Determination of the measurement uncertainty and evaluation of the performance parameters have been briefly discussed in the previous sections.

1.9 Conclusions and Future Work

An in-depth description is provided on the design of a time multiplexed dTDLAS-WMS OGS HCl spectrometer developed at PTB and testing using a surrogate gas. A novel bypass calibration scheme is presented, and a bypass manifold is designed for HCl to integrate the critical orifice device based dynamic gas standard from NPL. The spectrometer measures a noise floor of $(1 – 3) \times 10^{-4}$ for dTDLAS and $(3 – 4) \times 10^{-5}$ for the WMS measurements for the various multipass cells. For the 36 m cell, the Allan deviation plots predict a target OD of 4.26×10^{-8} cm^{-1} $Hz^{-1/2}$. This corresponds to an HCl detection limit of 380 ppt for 11 seconds of averaging time. A future measurement campaign will seek an equivalence between the dTDLAS/WMS optical gas standard developed at PTB with the dynamic reference standards developed in the WP2 of the project for intercomparison and consensus. The novel bypass calibration system will be evaluated to determine its calibration interval.

1.10 References

[1] O. Werhahn and Jan C. Petersen, "TILSAM - a technical protocol," 2010. [Online]. Available: https://www.euramet.org/technical-committees/tc-projects/details/project/gas-metrology-by-calibration-free-infrared-laser-spectrometry-as-a-potential-primary-method-traceab/?L=0&tx_eurametctcp_project%255Baction%255D=show&tx_eurametctcp_project%255Bcontroller%255.

[2] J. a Nwaboh, O. Werhahn, P. Ortwein, D. Schiel, and V. Ebert, "Laser-spectrometric gas analysis: CO2 –TDLAS

at 2 µm," *Meas. Sci. Technol.*, vol. 24, no. 1, p. 015202, 2013, doi: 10.1088/0957-0233/24/1/015202.

[3] N. Lüttschwager *et al.*, "*Traceable amount of substance fraction measurements in gases through infrared spectroscopy at PTB*," *17th International Congress of Metrology*, EDP Sciences. 2015.

[4] G. B. Rieker *et al.*, "A diode laser sensor for rapid, sensitive measurements of gas temperature and water vapour concentration at high temperatures and pressures," *Meas. Sci. Technol.*, vol. 18, no. 5, pp. 1195–1204, 2007, doi: 10.1088/0957-0233/18/5/005.

[5] T. Benoy, M. Lengden, I. Armstrong, D. Wilson, G. Stewart, and W. Johnstone, "Near IR tunable diode laser spectroscopy for aero engine research," 2014.

[6] G. B. Rieker, J. B. Jeffries, and R. K. Hanson, "Calibration-free wavelength-modulation spectroscopy for measurements of gas temperature and concentration in harsh environments.," *Appl. Opt.*, vol. 48, no. 29, pp. 5546–5560, 2009, doi: 10.1364/AO.48.005546.

[7] T. Fernholz, H. Teichert, and V. Ebert, "Digital, phase-sensitive detection for in situ diode-laser spectroscopy under rapidly changing transmission conditions," *Appl. Phys. B Lasers Opt.*, vol. 75, no. 2–3, pp. 229–236, 2002, doi: 10.1007/s00340-002-0962-0.

[8] A. Klein, O. Witzel, and V. Ebert, "Rapid, Time-Division Multiplexed, Direct Absorption- and Wavelength Modulation-Spectroscopy," *Sensors*, vol. 14, no. 11, pp. 21497–21513, 2014, doi: 10.3390/s141121497.

[9] T. Salthammer, "Formaldehyde in the Ambient Atmosphere: From an Indoor Pollutant to an Outdoor Pollutant?," *Angew. Chemie Int. Ed.*, vol. 52, no. 12, pp. 3320–3327, 2013, doi: 10.1002/anie.201205984.

[10] K. Wunderle, "TDLAS spectrometer for H2O boundary layer measurement of plant leaves."

[11] T. Benoy, Z. Qu, O. Werhahn, and V. Ebert, "Rapid Time division multiplexed dTDLAS and digital-correlative wavelength modulation spectroscopy (cd-WMS) in a Multipass Cell: A surrogate gas methodology using CO 2 gas at 2.7 um for dynamic gas standards," 2020.

[12] "Substrate selection guide." [Online]. Available: https://eagletube.com/resources/optimal-metal-tubing-for-medical/#:~:text=For medical implants%2C titanium tubing,in desalination and marine applications.

[13] D. A. Smith, Min Yuan, J. Bischof, L. Patterson, and J. B. Mattzela, "Amorphous silicon coatings for control of corrosion and metal ion contamination," pp. 352–356, 2017, doi: 10.23919/mipro.2017.7966606.

[14] "A guide for the selection of sample transport tubing" [Online] https://hrd1127ph3ye0og33luxdzon-wpengine.netdna-ssl.com/wp-content/uploads/2018/08/OBrien-Silcotek-Sample-Transport-Selection-Guide.pdf

[15] "Dursan ® and SilcoNert ® 2000 Coating Comparison Guide Game-Changing Coatings ™," p. 2000, 2000.

[16] BIPM, "GUM: Guide to the Expression of Uncertainty in Measurement." [Online]. Available: https://www.bipm.org/en/publications/guides/gum.html.

[17] A. Pogány, S. Wagner, O. Werhahn, and V. Ebert, "Development and metrological characterization of a tunable diode laser absorption spectroscopy (TDLAS) spectrometer for simultaneous absolute measurement of carbon dioxide and water vapor," *Appl. Spectrosc.*, vol. 69, no. 2, pp. 257–268, 2015, doi: 10.1366/14-07575.

[18] A. Pogány *et al.*, "Metrology for ammonia in ambient air – concept and first results of the EMRP project MetNH3," vol. 3, p. 07003, 2015, doi: 10.1051/metrology/201507003.

[19] A. C. (NPL), "Deliverable D7: Specification for the Metrology of Airborne Molecular Contaminants."

2 Mid-IR cavity ringdown spectroscopy - VSL

2.1 Experimental set-up at VSL: OPO-based mid-IR CRDS

VSL operates a spectrometer based on mid-infrared Cavity RingDown Spectroscopy (CRDS) which has been described before in detail [0]. For the MetAMC II project this system has been optimized for the detection of HCl at trace levels. Therefore, here only a short description of the system is provided with an emphasis on the key points for rapid and sensitive HCl detection.

Figure 2.1 shows a schematic overview of experimental setup based on a continuous wave (cw) optical parametric oscillator (OPO) as light source and CRDS used for the gas detection. The pump laser of the OPO consists of a narrow line-width cw fibre laser (NKT Photonics, output power set at 4.4 mW) which is amplified in a fibre amplifier (IPG Photonics). This combination provides a wide mode-hop-free tuning range of 100 GHz and an output power up to 10.5 W at 1064 nm. The output of the amplifier is coupled into the OPO cavity () bow-tie configuration) via a collimator (COL), Faraday isolator (FI), and an AR-coated focusing lens (L1). The periodically poled crystal (PPLN) from HC Photonics is contained in an oven and has AR coatings for signal, pump, and idler wavelengths. The mirrors are highly transparent for both idler and pump wavelengths and highly reflective for the signal wavelength. The backside of the mirrors is antireflective coated for both the pump and idler. Within the PPLN crystal, the pump light is converted into the signal and idler with the signal resonating in the OPO cavity.

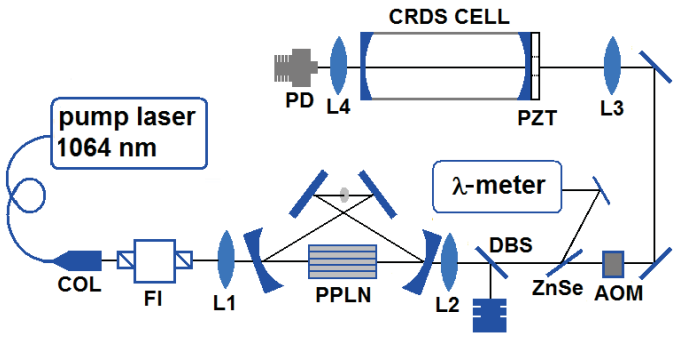

Figure 2.1 Schematics of the singly resonant cw OPO. The output of the seed fibre laser is amplified up to maximum 10.5 W and coupled into the OPO cavity. Part of the idler is directed to a wavelength meter and the rest is directed via an Acoustical Optical Modulator (AOM) to the cavity ring down measurement cell.

The output of the OPO is collimated using an uncoated CaF_2 lens (L2). Signal and residual pump are separated from the idler using a dichroic beam splitter (DBS). Part of the idler beam is directed to a wavelength meter (Bristol instruments) using a ZnSe window placed near the Brewster angle.

The key steps in order to reach the high sensitivity and fast time response for HCl are:

- ✓ **Selected wavelength region**

  The wavelength region of the OPO covers the entire fundamental ⍰$_1$ –band containing many strong absorption lines. Here we selected the strongest $H^{35}Cl$ line of this band, the R(3) line; this line is centered at 2963.2853 cm^{-1} and has a line strength S of $4.856 \cdot 10^{-19}$ cm^{-1} /molecule cm^{-2} according to HITRAN database. This line is about 3 times stronger than the neighboring $H^{37}Cl$ line at 2961.0679 cm^{-1} ($S=1.55 \cdot 10^{-19}$ cm^{-1} /molecule cm^{-2}) due to the about 3 times higher abundance

of ^{35}Cl. Fortunately, one of the CRDS mirrors set available at VSL provides a very high reflectivity for the mid-IR region of ca 99.99% at 2963.2853 cm^{-1} giving rise to a decay time up to 17.5 µs in the absence of an absorbing gas. This corresponds to an effective absorption path length of 5.25 km. In the atmosphere the main spectrally interfering components are water and, in lesser extent, methane. By measuring at a reduced cell pressure (100 mbar or lower) the H_2O interference can be effectively reduced. In the experiments presented here, HCl was measured in a relatively dry nitrogen matrix and therefore the measurements could be performed at pressures near atmospheric.

✓ **Choice of passivation treatment (CRDS cell, mass flow controller & tubings)**

HCl strongly reacts with many different materials. VSL studied the interaction of HCl with various polymers, metals, and coated metals within the framework of this project [0]. Most polymers and coated metals showed good performance for HCl while uncoated metals were found to be unsuitable. In the present work we used only SilcoNert® 2000 coated stainless steel (CRDS cell, mass flow controller and tubing) to reduce the HCl surface interaction as much as possible while at the same time not admitting moisture to the system as would be the case when polymers are being used.

2.2 HCl reference gas mixtures prepared using a magnetic suspension balance

Low amount fractions of HCl for the validation of the instrument performance were generated following ISO6145-10 [1] using a permeation system based on a magnetic suspension balance (MSB) [1]. A permeation tube (manufacturer Fine Metrology) was used to generate low amount fractions of HCl (see Figure 2.2). This permeation tube was specified by the manufacturer to have a permeation rate of 39 ng/min (±5%) at 30.0 °C. The MSB records the mass of the permeation tube at high time resolution and the mass loss rate of the tube is determined by using a linear fit of the mass as a function of time. The MSB was operated at a low temperature of 15 °C in order to get as low amount fractions as possible. Later, a lower temperature of 10 °C was used in order to reach even lower amount fractions but condensation occurred on the MSB leading to spurious readings (Based on the 45% relative humidity and 20 °C laboratory temperature a minimum temperature of about 8 °C was anticipated). A small nitrogen flow of 50 ml/min was passed though the permeation chamber. The exiting flow containing the permeated HCl was diluted with a much larger nitrogen flow up to 5 L/min.

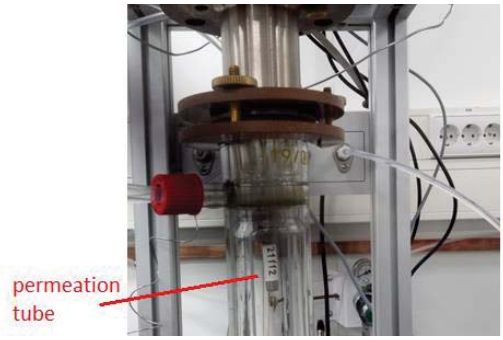

Figure 2.2 HCl permeation tube inside the permeation chamber of the MSB.

HCl amount fractions in the low nmol/mol till a few hundred nmol/mol can be generated with this system. Figure 2.3 shows an example of the mass loss rate determined for 2 low temperatures of the permeation tube.

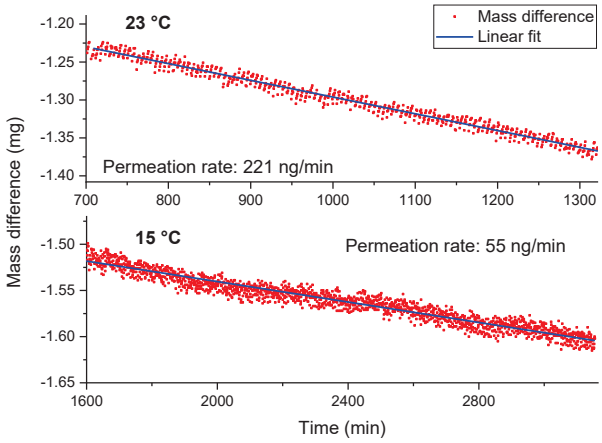

Figure 2.3 Mass lose rate of the HCl permeation tube determined at 23 °C (upper panel) and 15 °C (lower panel).

Small part (about 12 L/h) of the HCl gas mixture from the MSB is led via a ca 5 meter SilcoNert® coated tubing (1/8 inch outer diameter) via a mass flow controller to the CRDS spectrometer (the rest of the gas mixture is sent to a vent). The pressure in the CRDS cell is kept at a constant pressure of 1000 mbar.

2.3 Results HCl measurements by OPO-based mid-IR CRDS

Figure 2.4 shows an example of the measured decay time for the R(3) transition of $H^{35}Cl$ at different amount fractions (range 2-19 nmol/mol). The use of high reflectivity mirrors leads to a high decay time and thus a high sensitivity of the CRDS spectrometer.

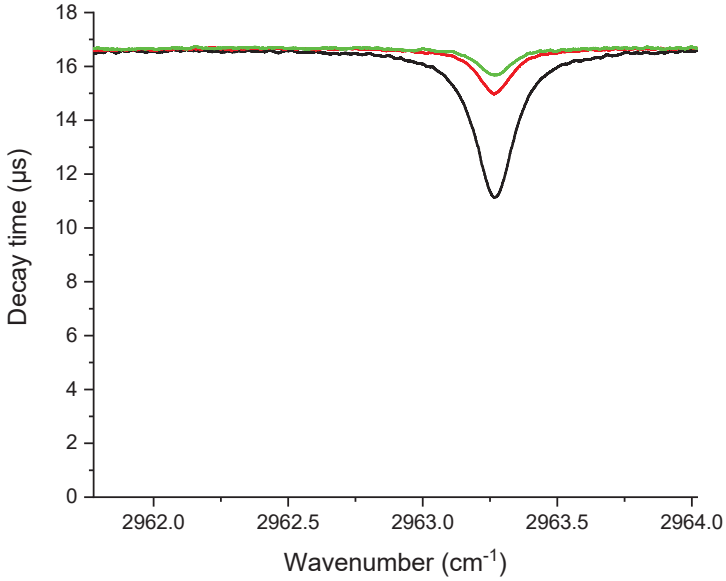

Figure 2.4 Measurement of the decay time for the R(3) transition of $H^{35}Cl$ at different amount fractions (calculate range 2-19 nmol/mol based on the Hitran line strength) at a cell pressure of 1000 mbar. The HCl was generated by permeation.

From the measured decay time the absorption spectrum can be calculated. Figure 2.5 shows two examples of the absorption spectra and the corresponding fit using a Voigt profile. From the absorption spectra the HCl amount fraction can be derived using the known line strength from Hitran. Doing this, significantly lower amount fractions of HCl are obtained than derived from the MSB. Therefore, it is expected that the permeation tube also emits some other compounds like H_2O (research to investigate this is currently in progress at VSL).

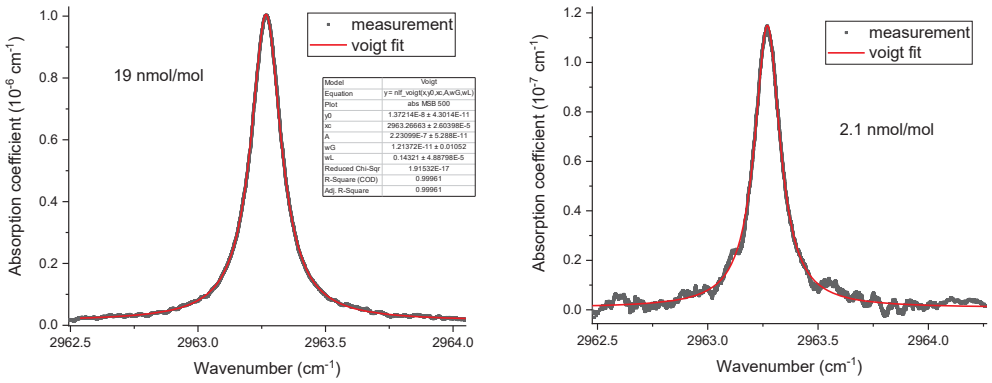

Figure 2.5 Derived absorption spectrum of HCl at a relatively high amount fraction ((left panel, derived amount fraction using lines strength is 19 nmol/mol) and low (2.1 nmol/mol, right panel). Both peaks can be well fitted with a Voigt profile. From the right panel a LoD below the targeted 1 nmol/mol can be derived.

Time response of the system:

For the system previously flushed with nitrogen, applying a step change in HCl amount fraction at low nmol/mol level, it takes less than 5 minutes to reach 95% of the final response. As the HCl has to flow through about 5-meter-long tubing the actual response of the analyzer will be faster. Note that based on the cell volume (about 100 ml) and applied flow rate (12 liter per hour) the CRDS cell is refreshed about once every 30 seconds). For a step down in concentration the response time was measured to be about similar.

2.4 Conclusion results VSL

It has been shown that the CRDS system is capable of detecting HCl at low levels with a limit of detection below the target level of 1 nmol/mol. Further improvements in sensitivity can be made by increasing the cell length. By reducing the cell diameter (currently 10 mm), the total cell volume can be kept small in order to reduce the time response of the system. An alternative way to boost the sensitivity is to use the recently developed single-crystal mirror coatings (developed by Crystalline Mirror Solutions which was recently acquired by Thorlabs). Such mirrors might provide even better reflectivity (thus lower HCl detection limits) than the mirrors used here based on ion-beam sputtering but their cost is currently still prohibitively high, yet this might change in the future with the wider uptake of this technology.

Some issues require further research.

I. A small absorption peak of HCl is present (corresponding to about 0.5 nmol/mol) when analyzing high purity nitrogen (either nitrogen BIP-plus from Air Products or from evaporated liquid

nitrogen). When looking at spectral databases like Hitran no likely candidate could be identified. It could be that both the nitrogen gases contain some HCl but this is not expected. Further, it could be that still some HCl is present from previous experiments, but this is also not so likely as HCl rapidly decreases as one switches from a HCl mixture to nitrogen.

II. The amount fractions from the MSB are significantly higher than the amount fraction derived using the line strength from Hitran. This is possibly caused due to some impurity (like H_2O) being released from the permeation tube. Currently we are trying to quantify the H_2O loss from HCl permeation tubes but this is quite challenging. It could also be that HCl is lost in the system, but this is less likely as the system responds quite rapidly to even a small step change in concentration. An alternative for using the MSB would be to dilute the HCl gas mixtures (as prepared by VSL within the framework of the MetAMC II project) to lower amount fractions using a 2-stage dilution system.

2.5 References

[1] Persijn, S. (2018). Purity analysis of gases used in the preparation of reference gas standards using a versatile OPO-based CRDS spectrometer. *Journal of Spectroscopy*, *2018*.

[2] van der Veen, A. M.H, Nieuwenkamp, G., Zalewska, E. T., Li, J., de Krom, I., Persijn, S., & Meuzelaar, H. (2020). Advances in metrology for energy-containing gases and emerging demands. *Metrologia*.

[3] http://empir.npl.co.uk/metamcii/wp-content/uploads/sites/43/2019/11/Sampling-lines-for-HCl-measurements.pdf

[4] ISO 6145-10, Gas analysis - preparation of calibration gas mixtures using 1645 dynamic volumetric methods - Part 10: Permeation methods. ISO, International Organization for Standardization, Geneva, Switzerland, First edition 2002.

3 MOPA powered photoacoustic spectroscopy - VTT

Due to copyright issue, this part has been removed

4 Multi-pass cantilever- enhanced photoacoustic spectroscopy - Gasera®

4.1 Theory

Photoacoustic spectroscopy is based on gas molecules absorbing the energy of infrared light. When the gas absorbs energy, it heats up and expands, which creates pressure increase in an enclosed space. When the infrared radiation is modulated with a certain frequency, the pressure variation in the photoacoustic sample chamber creates an acoustic wave of the same frequency. The light energy is converted into pressure variations i.e. sound energy, which is then converted into electric signal using a microphone.

Major advantage of the photoacoustic effect in gas analysis is that sensitivity is independent on the absorption path length. This allows high sensitivity (sub-ppb) with a short absorption path length and highly linear response over a wide dynamic measurement range from very low sample volumes (typically few milliliters). This key feature also provides the potential for miniaturization to hand-held size without losing its laboratory-grade sensitivity.

In the applications of photoacoustic spectroscopy, the sensitivity of a microphone is one of the most critical parameters and some applications, such as trace gas analysis, demand the highest sensitivity. Gasera has developed a novel MEMS cantilever approach to detect pressure changes in a photoacoustic cell [2]. High sensitivity is achieved by using a patented cantilever pressure sensor which is more than hundred times more sensitive than a membrane microphone, which is conventionally used in photoacoustic spectroscopy.

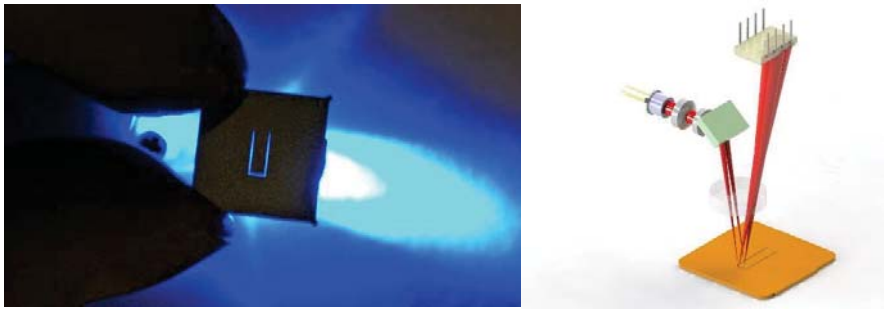

Figure 4.1 Cantilever sensor and readout interferometer

An extremely thin cantilever portion moves like a flexible door due to the pressure variations in the surrounding gas. The displacement of the cantilever is measured with an accurate interferometric readout system. This way we can avoid the so-called “breathing effect”, which occurs in capacitive measurement principle where the other electrode damps the movement of the sensor and restricts the dynamic range. Gasera’s patented laser-based readout interferometer can accurately measure displacement from well under a picometer up to millimeters.

The cantilever sensor is made from single crystal SOI-silicon with a specially developed dry-etching process that leads to a highly stable and robust component; therefore, the sensor is practically totally immune to temperature and humidity variations. In addition, the sensor does not suffer from wearing. Furthermore, the sensor and readout can be isolated in terms of temperature allowing heated gas cell which enables applications that require gas analysis at elevated temperatures such as chemical emissions monitoring and process control.

4.2 Gas species and line selection criteria

The gas sensor developed by Gasera measures HCl and H2O using a single interband cascade laser (ICL). Gasera chose to investigate an HCl transition near 3374.6 nm (as shown in figure 4.2) as the optimal HCl transition for their device development. Please note that the top part of the figure shows the simulated wavelength modulation absorption spectrometry (WMAS) signal which is used in the analysis. The lower part shows the conventional absorption spectrum for reference. It was chosen because of high line strength, availability of DFB interband cascade lasers (ICLs) from Nanoplus (https://nanoplus.com/en/news/icl-3000-6000-nm/) and moderate spectral interference from H_2O. Please note that the figure has 10 ppb of HCl in ambient (1.2 % H_2O ~50 RH normal temp) gas matrix. Initial tests of the Nanoplus ICL show that it does not have the best spatial mode quality.

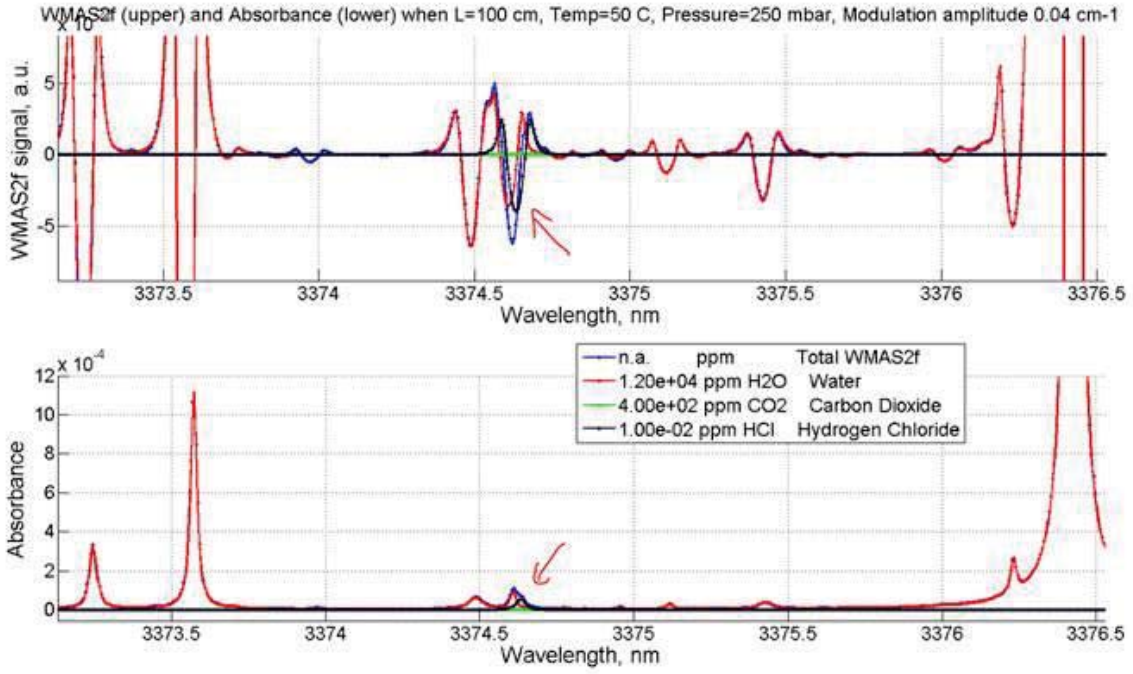

Figure 4.2 Modelled WM-PAS spectroscopy signal (top) and absorbance (bottom) of HCl and potential cross-contaminants (Gasera).

4.3 Optical configuration and experimental setup

As explained in the second progress report (period from 1 February 2019 to 31 October 2019), Gasera had issues with optical feedback in the new multipass optical configuration. The mitigation plan was to simplify the optical configuration and to use a new structure based on a double pass configuration. The unit was built based on a double pass configuration which virtually eliminated all optical feedback related effects. The downside is that the sensitivity will not be as good as expected, because the total optical power inside

the photoacoustic cell is not a high as it would have been with e.g. a multipass configuration with six passes.

The used structure is based on the model shown in the figure below. The ICL is mounted inside the cylindrical structure at the top left part of the figure 4.3. Optical multipass configuration (double pass) is achieved by positioning a mirror at the end of the photoacoustic cell, which is marked by 3 in the figure. The golden mirror in structure 2 reflects the beam exiting the photoacoustic cell into a thermal power sensor.

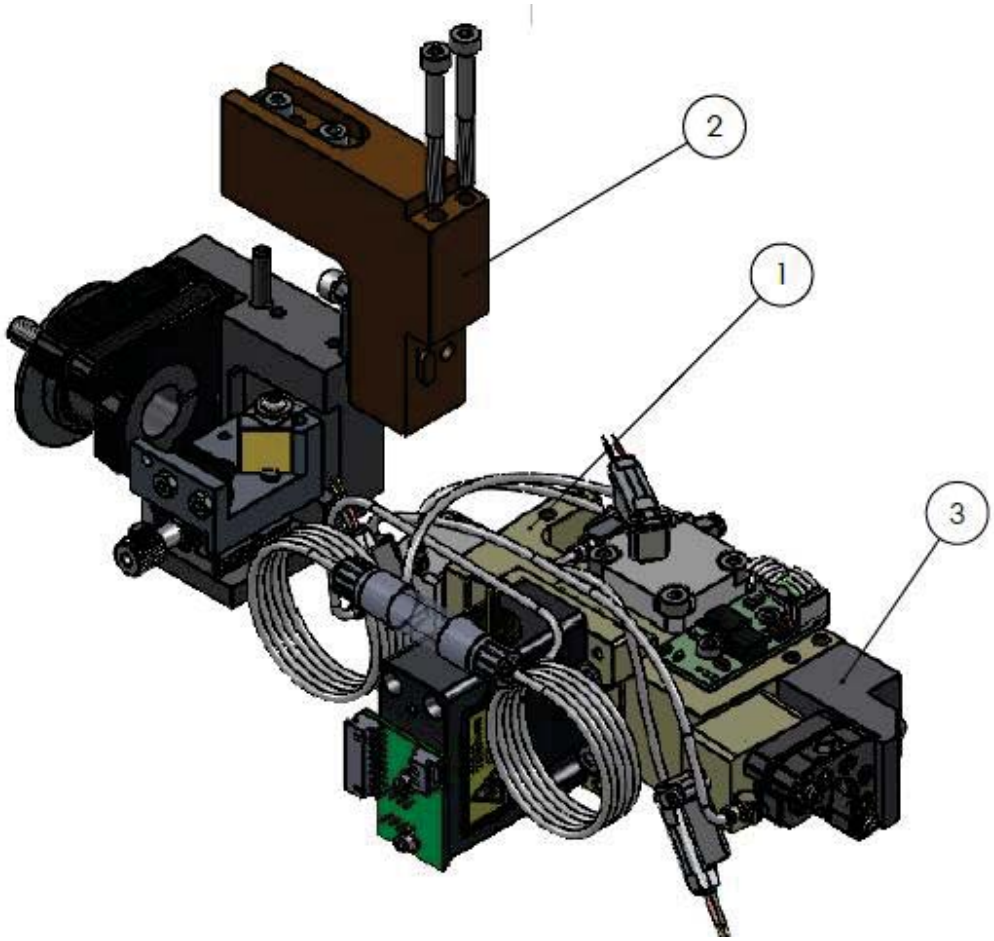

Figure 4.3 Gasera's optical multipass (double pass) structure. 1) Photoacoustic cell, 2) holder for the laser mount and 3) double pass feedback mirror holder.

Gasera's experimental setup is very simple: gaseous sample is generated by mixing HCL (in N2 balance) from a cylinder with synthetic air. The mixing is done using two Brooks SS MFCs. In addition, humidity was added to the system by mixing the dry and diluted HCl flow with another controlled from a bubbler.

4.4 Gas sampling system

The gas sampling system used in Gasera's developed system is shown in figure 4.4. The path marked with dashed green line shows the path of the gas from input 1 (under V1) to the pump and out from the SAMPLE

OUT. The tubing between V1 and the cell is PTFE or PVDF. In a standard gas exchange, the cell is first flushed with sample and then evacuated to a measurement pressure of 200 mbar by closing the valve before the cell and by monitoring the pressure using the pressure sensor. The tubing diameter between the measurement cell and the V1 (valve 1) is 2 mm.

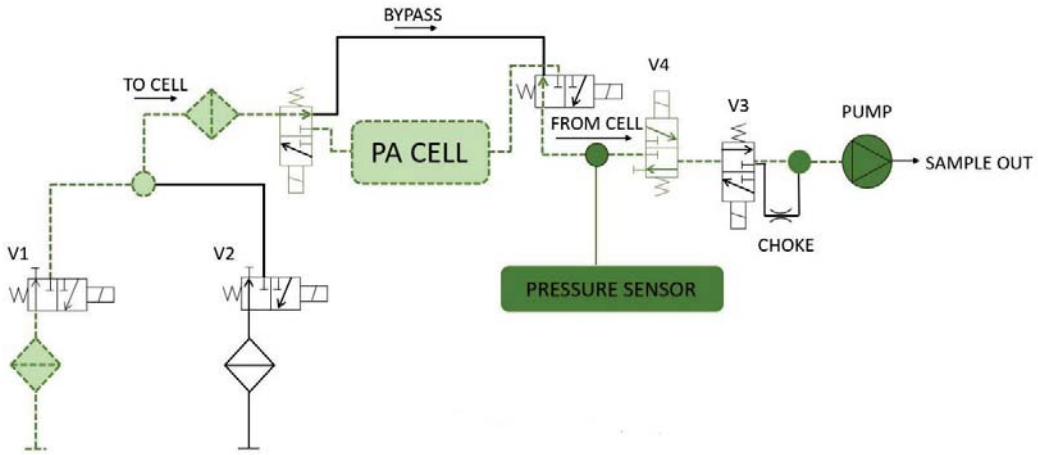

Figure 4.4 Gasera's internal gas handling configuration.

4.5 Recommendations to instrument operation

Photoacoustic principle always requires a calibration, since the photoacoustic response originating from the absorption of the light by the sample gas molecules is not that well defined.

4.6 Standard tests (please refer to the recommendations for lab and field testing,) and results

The unit was configured to have a 37 sec time between the samples. The sample time comprises of gas exchange time and the actual measurement time. Since the measurement is a "sample-and-hold" type of a measurement, the chose time is a compromise between response time and sensitivity.

Detection limit can be determined by calculating the noise at zero. Another way is determining the detection limit would be to calculate the noise at some non-zero HCl concentration. The following figures show the zero and 950 ppb measurements.

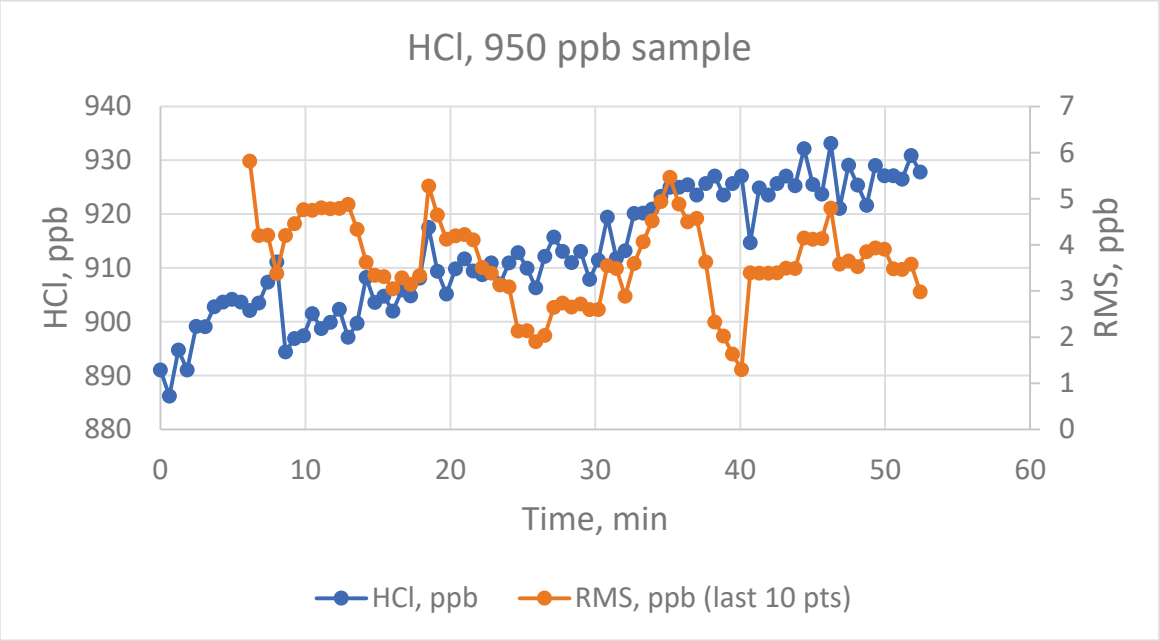

Figure 4.5 950 ppb HCl measurement using Gasera's photoacoustic unit

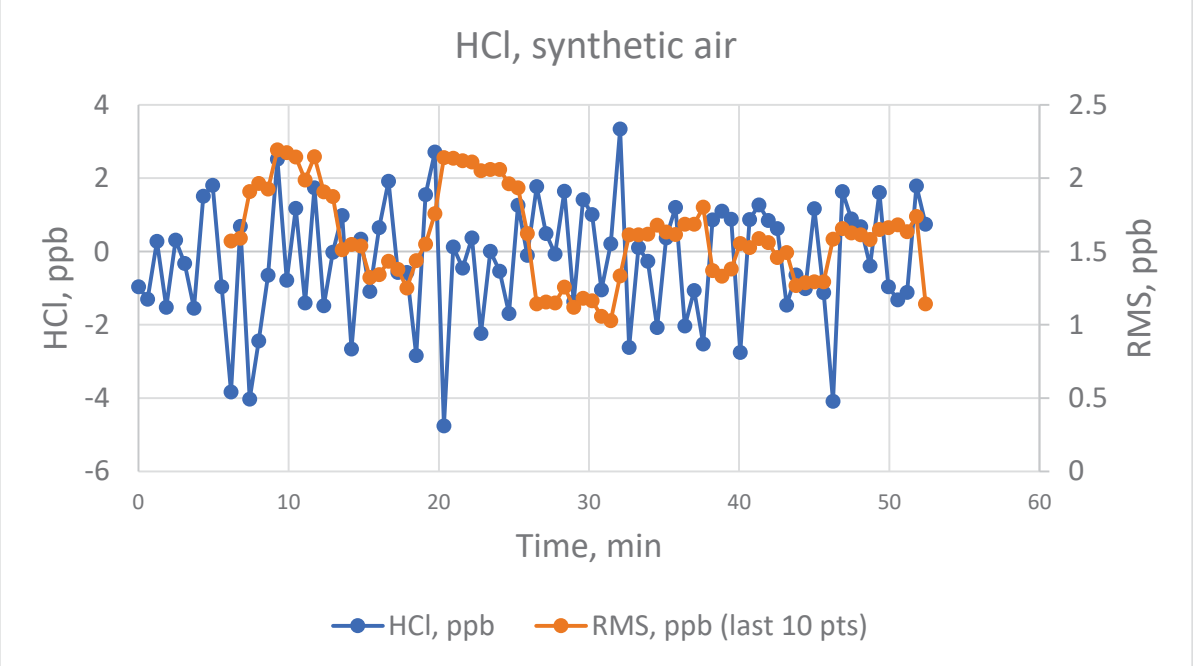

Figure 4.6 Zero air (synthetic air) HCl measurement using Gasera's photoacoustic unit

Standard deviation, or LOD, of HCl in the zero-air measurement is 1,62 ppb (or nmol/mol) using a sample time of 37 seconds. The LOD normalized to 60 second sample time is 1,27 ppb (or nmol/mol). One can see from figure 4.6 that there is a slight drift in the readings by looking at the orange line. One can also see that there are sections where the RMS is just below 1 ppb, which would put the 60-second LOD just under 1 ppb

(or nmol/mol). The LOD determined from the figure 4.5 would be probably about a factor of two higher than the LOD determined from the zero measurement. The higher LOD is partly because of unstable HCl concentration due to sorption effects and also because of higher relative signal noise due to high HCl level. One should note that the relative noise in the 950-ppb measurement is approximately 0.4 % (4 ppb / 950 ppb) which is low and close to being limited by the stability of the photoacoustic sensor.

Response time of the developed system was verified by generating sample of zero air and 7.5 ppm HCl samples periodically in a stepwise manner. The results are shown in figure below.

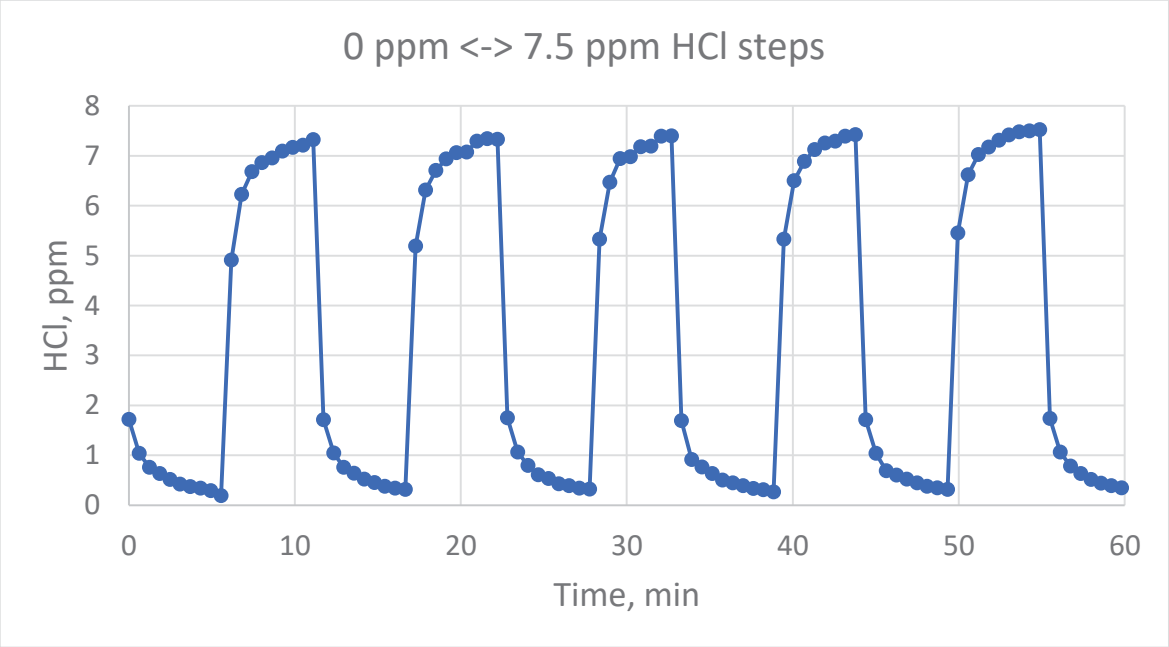

Figure 4.7 Response time test using Gasera's prototype

The response time (10/90) is in the order of 2 minutes. The sample time in the measurement is 37 seconds.

4.7 Conclusions

Gasera developed a photoacoustic sensor prototype for HCl with a sensitivity in the order of 1 ppb (nmol/mol) using a sample time of 60 seconds. The response time is in the order of 2 minutes when using zero air and 7.5 ppm levels as the low and high levels, respectively. Gasera 's photoacoustic sensors always require a calibration, because the photoacoustic principle in not an absolute optical detection method.

4.8 References

[1] J. Kauppinen, K. Wilcken, I. Kauppinen, and V. Koskinen, "High sensitivity in gas analysis with photoacoustic detection," Microchem. J. 76, 151-159 (2004)

5 Noise-immune cavity-enhanced optical heterodyne molecular spectroscopy (NICE-OHMS) - NPL

5.1 Theory

In frequency modulation (FM) spectroscopy [1], laser light is modulated using an electro-optic phase modulator (EOM). This light is transmitted through an absorbing medium (Figure 5.1) imaged onto a fast photodiode. The detector output is directed to a double balanced mixer (DBM); the DBM reference channel is a copy of the modulation frequency but shifted in phase from the signal to the modulator.

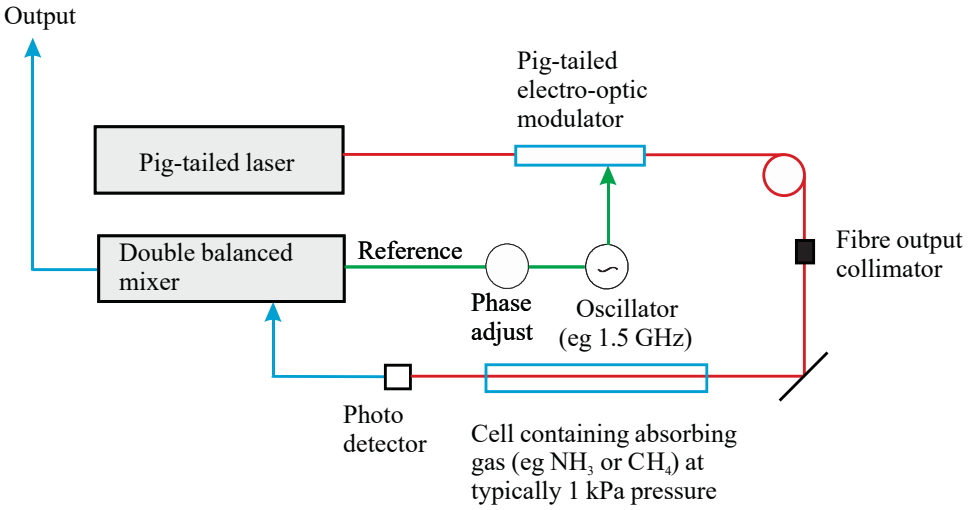

Figure 5.1 Schematic of an FM spectroscopy arrangement.

If the absorber attenuates the carrier and sidebands equally, then no amplitude modulation results, and a minimal DC output signal is observed from the mixer. However, as the laser is tuned towards a linear absorption, the sidebands become imbalanced in terms of their intensity and the resulting amplitude modulation is observed as a DC signal at the mixer output. The theory was established in [1] and the output signal χ as a function of frequency detuning $\Delta\nu$ from line centre can be written as:

$$\chi(\Delta\nu) = hP_0\alpha_0 L J_0(\beta)J_1(\beta)[\{\chi^{abs}(\Delta\nu-\nu_m)-\chi^{abs}(\Delta\nu+\nu_m)\}\sin\theta + \{\chi^{disp}(\Delta\nu-\nu_m)-2\chi_{disp}(\Delta\nu)+\chi^{disp}(\Delta\nu+\nu_m)\}\cos\theta \quad (5.1)$$

Here, J_n is a Bessel function of order n, with modulation index β. The modulation frequency is ν_m and the phase between the modulation frequency at the modulator and the mixer is given by θ. The incident laser power is denoted by P_0; the effective path length is L and the absorption factor α_0. Whilst in [1], a Lorentzian spectral profile was assumed, the equation above has been generalised to include an arbitrary profile χ; note that this function is complex with the real and imaginary components corresponding to absorption and dispersion signals respectively. Examples of common lineshape functions were published in [2].

The NICE-OMHS technique was first demonstrated over 20 years ago [3]. In this cavity-enhanced version of FM spectroscopy, the cavity free spectral range is matched to the modulation drive frequency. A simplified NICE-OHMS schematic is shown in figure 5.2; in this example, a 10-cm cavity is used together with a 1.5 GHz modulation frequency. In this figure 5.2, the NICE-OHMS signal is observed via the detector in transmission; the detector monitoring reflected light is used both for locking the laser to the cavity and for generating the "Devoe-Brewer" (DVB) signal that is used to servo the modulation frequency to the free spectral range [4]. For some years, it was assumed that equation (1) described the NICE-OHMS just as well as it did for FM spectroscopy. However, in recent years it has become clear that this is a generally unjustified simplification and an improved theory has been developed [5, 6]. These papers describe how phase shifts introduced by the absorber within the cavity lead to changes in the observed NICE-OHMS profile. The dependency on signal size as a function of concentration then becomes non-linear, as observed [7]; also see Figure 5.3.

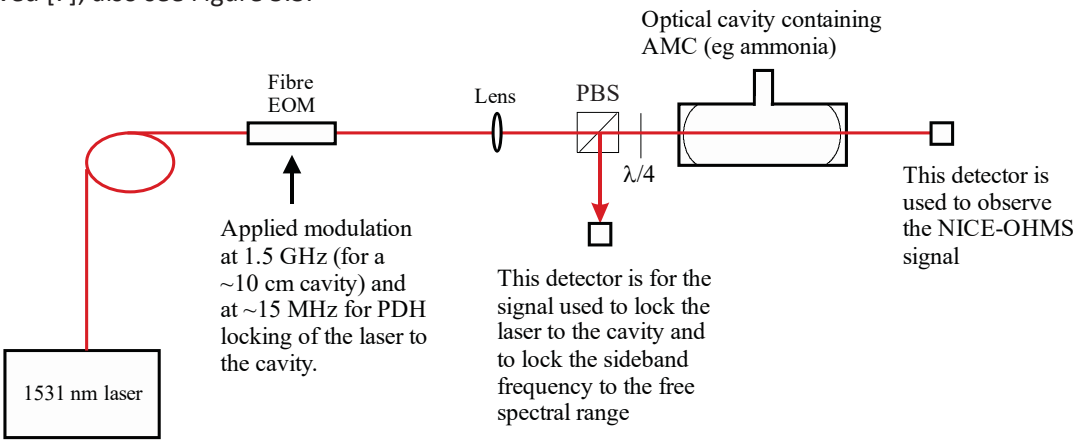

Figure 5.2 Simplified NICE-OHMS schematic.

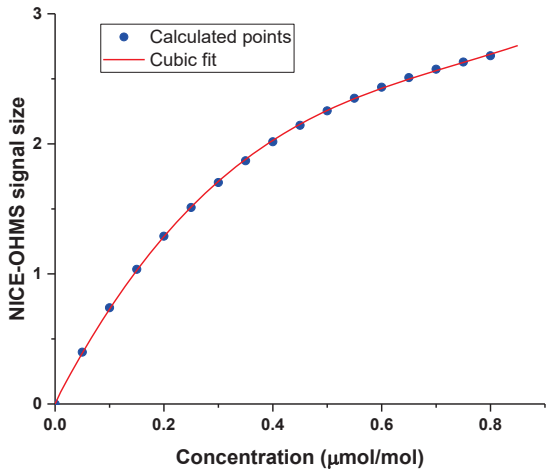

Figure 5.3 Calculated NICE-OHMS signal using the ELFT approximation (see text). A cubic fit to the calculated discrete points is also shown.

In the theory developed in [5], equation 1 is referred to as the "CONV" (conventional) expression for the NICE-OHMS signal. This is valid only for the case of weak linear absorption; whether the absorption is "weak" is characterised via the parameter $\kappa = F\alpha_0 L/\pi$ where the cavity finesse is *F*, single-pass length *L*

and absorption coefficient α_0. In cases where κ<0.1, the "CONV" expression is adequate, but for higher κ, either the "ELET" (extended locking and extended transmission) or "ELFT" (extended locking and full transmission) approximations need to be used. It is shown that these successive approximations are valid for $\kappa \lesssim 0.3$ and $\kappa \lesssim 0.6$ respectively. Both these are closed-form solutions although are increasingly difficult to code and test. There is also a "FULL" solution described in [5] for $\kappa \gtrsim 0.6$ that cannot be written in closed form and requires solving a set of non-linear equations.

As an example, the NICE-OHMS signal at 1742 nm is calculated at different concentrations in figure 5.3; here the ELFT approximation was assumed. The calculation is for a 10-cm cavity (≡1499 MHz modulation frequency) of finesse 169,000; a Voigt profile is assumed and the RF phase set to 90°. The HCl is assumed to be in dry air (nitrogen) at 101.3 kPa pressure (one atmosphere).

In addition, the calculated points have been fitted to a cubic to allow more straightforward calculations of the concentration from an observed NICE-OHMS signal size. Although in [7] an exponential function was fitted to the results, polynomial fits are simpler both to fit and invert. Over the limited concentration range of figure 5.3, both assumed functional forms work well.

5.2 Gas species and line selection criteria

In order to physically construct a NICE-OHMS system to detect HCl at the ppb level, we need to address the trade-off between different aspects of developing such a device, wavelength dependence on maximum signal size, commercial availability of components, including lasers, modulators, optics and detectors (or our ability to design and produce components), and overall size and portability of the final device.

There are a number of spectroscopic windows available with strong enough line intensities to enable detection of HCl by NICE-OHMS at ultra-low concentrations (ppb regime), see figure 5.4. To choose between these we consider what is required to design and execute a compact and low-maintenance NICE-OHMS-based system. In the first instance, fibre-based components are preferred, to minimise changes to alignment of this optical system.

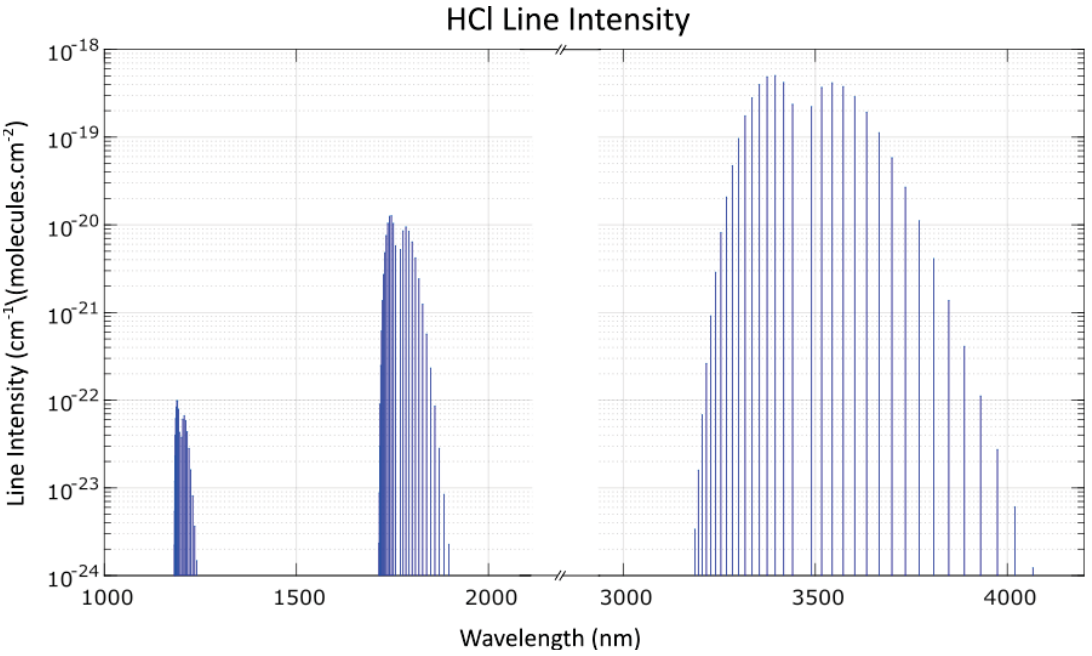

Figure 5.4 HCl line intensity plot showing three regions of interest for laser spectroscopic methods of detection; data from HITRAN.

Another consideration unique to the high-finesse cavity system of NICE-OHMS, is the need to choose a spectral region in which ultra-high reflectivity mirrors can be fabricated. At the selected detection wavelength, we require a compact laser system, preferably fibre coupled, and providing isolation between the laser output and the fibre interface, that is, interior to the laser packaging. Finally, it is necessary to modulate the frequency of laser in order to create sidebands on the light at the free spectral range of the cavity enclosing the sample. To maximise signal size, the ideal modulation frequency would be approximately at the HWHM of the absorption feature being probed; in our case this is of the order of 1 GHz. Additionally, the length of the cavity, combined with the reflectivity of the mirrors, produces the effective path length of Equation 1, but the requirement for a compact system suggests we should minimise the size of the cavity and cavity enclosure. We have therefore compromised with an approximately 10 cm-long cavity, with a corresponding need for modulation frequency of ~1.5 GHz. Direct modulation to the laser diode at these high frequencies is difficult and can produce amplitude modulation an unacceptable level, leaving us with the option of using an electro-optic modulator (EOM). Fibre-coupled EOMs for laser output modulation are not available in certain wavelength regions and are not yet widely produced for application at wavelengths above ~2.2 microns. Also, the commercially available fast detectors needed for the demodulation techniques used in NICE-OHMS are also limited to wavelengths of around 2 microns or less. These restrictions and limitations have led us to choose to work in the wavelength window below 2000 nm. We have specifically chosen to excite the transition at 1742 nm (5739.25 cm^{-1}), where both sufficiently powerful DFB lasers, high reflectivity mirror coatings, fibre-coupled EOMs, and fast detectors can all be commercially sourced. However, for concentrations of HCl at less than 100 ppb, additional concern is merited by the presence of water vapour lines near the 1742 nm transition. For non-dry environments, there is a concern that the tail of a water vapour feature might interfere with our NICE-OHMS detection at ultra-low concentrations, as shown in figure 5.5. Careful

modelling of the HCl NICE-OHMS feature in the presence of water at various concentrations and experimental evaluation might be necessary to address this issue.

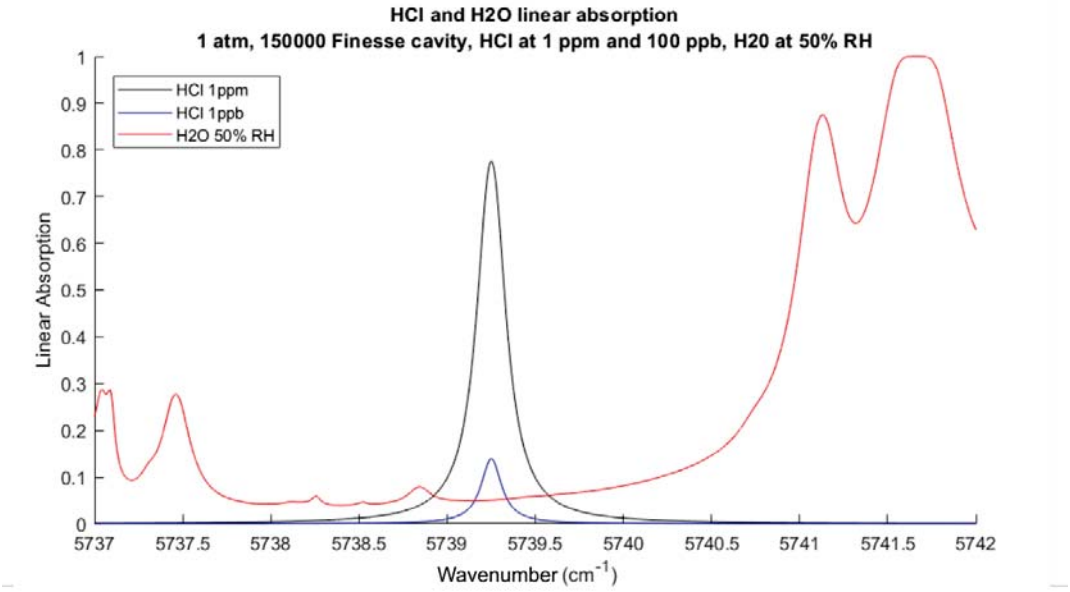

Figure 5.5 Calculated overlay of HCl and water vapour absorption near the HCl 1742 nm line (5739.25 cm^{-1}) as chosen for our proposed NICE-OHMS system.

5.3 Low noise current drivers

Mode matching of the output from the DFB laser with the optical cavity is essential in achieving efficient coupling. Ideally the laser beam would couple entirely to the fundamental spatial mode (TEM_{00}) of the cavity and into none of the higher order traverse modes [8]. To do this, the waist size and position of the beam should be well matched to the parameters calculated for the cavity [9]. For Gaussian beams, we evaluate a 1/e amplitude radius [9] which can be calculated from the cavity length and mirror radii of curvature – note in our case we utilise the same plano-concave laser cavity [10] that was used in the MetAMC project [7]. For high finesse cavities the linewidth is much smaller than that of the input laser [11]. Therefore, the laser output will naturally be attenuated when coupling with the cavity. As a result, it is critical that linewidth broadening due to technical noise (e.g. that generated by a noisy current driver) is minimised.

Since the semiconductor diode laser output frequency is dependent on the injection current, reducing the electrical noise from the laser diode current driver in turn reduces the laser linewidth. Using low noise digital current drivers based on a Hall-Libbrecht design [12, 13], it is shown that the beat between two identical diode lasers is improved in terms of linewidth and frequency jitter, when compared using commercial current controller devices to drive the lasers.

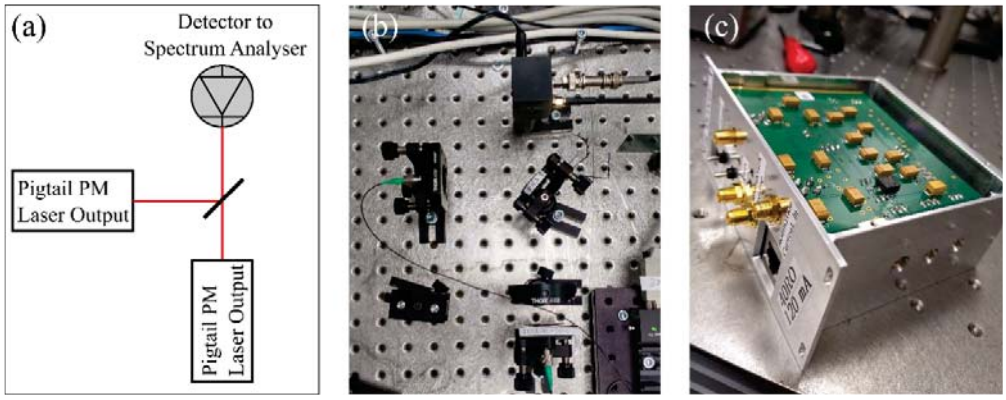

Figure 5.6 (a) Schematic and (b) optical layout for beat measurements between two pigtailed DFB lasers. (c) Digital low noise current driver based on Hall-Libbrecht design.

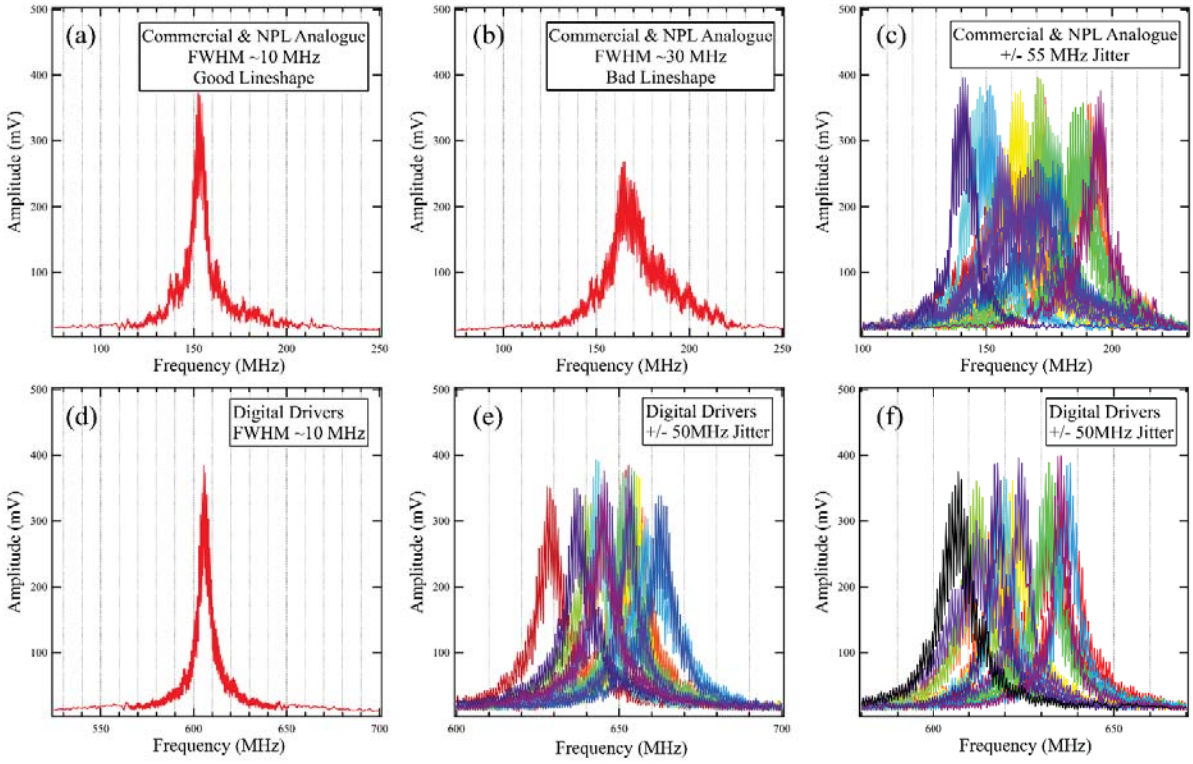

Figure 5.7 Resultant beats from Eblana 1742 nm DFB lasers. Using a commercial current driver and NPL analogue current driver the beat is unstable in linewidth and fluctuates between (a) a narrow FWHM and (b) broadened FWHM and experiences (c) frequency jitter. The low noise digital current drivers exhibit (d) a consistently narrow linewidth and similar jitter (e) and (f).

The laser linewidth is determined as the half width half maximum (HWHM) of an optical beat produced by two identical lasers. Using lasers centred at 1742 nm (1854 nm), the wavelength intended for molecular hydrogen chloride (water) spectroscopy, the full width half maximum of the optical beat is measured using an RF spectrum analyser as shown in figure 5.6. It is essential that there is isolation between the laser

and the optical system, to reduce optical feedback, which broadens the laser spectrum. It should be noted that the 1854 nm pair of lasers have two in-built isolators within the butterfly mount whereas the 1742 nm pair only has one in-built isolator and an additional fibre-based isolator has been added externally to the beam path to further reduce feedback to the laser diode.

To evaluate the digital driver performance the resultant beats produced using the low noise digital current drivers is compared against two Eblana 1742 nm lasers driven with various drivers. Figure 5.7 compares the beats produced using (a-c) a commercial and NPL analogue current driver configuration and (d-f) the low noise digital drivers. Figure 5.7a and d compare a "good" representative beat from both drivers and a FWHM of 10 MHz. However, the overall signal noise and especially noise at the wings of the lineshape are markedly improved. In addition to this, the overall stability of the lineshape is improved. Figure 5.7b shows that the beat lineshape can significantly broaden (FWHM =30 MHz) when the lasers are not driven with digital drivers. Figure 5.7c, e and f compare continuously sampled beats in each configuration to demonstrate reproducibility. It is clear that the digital drivers consistently improve the stability of the lineshape, and also reduce frequency jitter. It should be noted that frequency jitter is not removed entirely, and the average central frequency is not stable over time; see figure 5.7e and f.

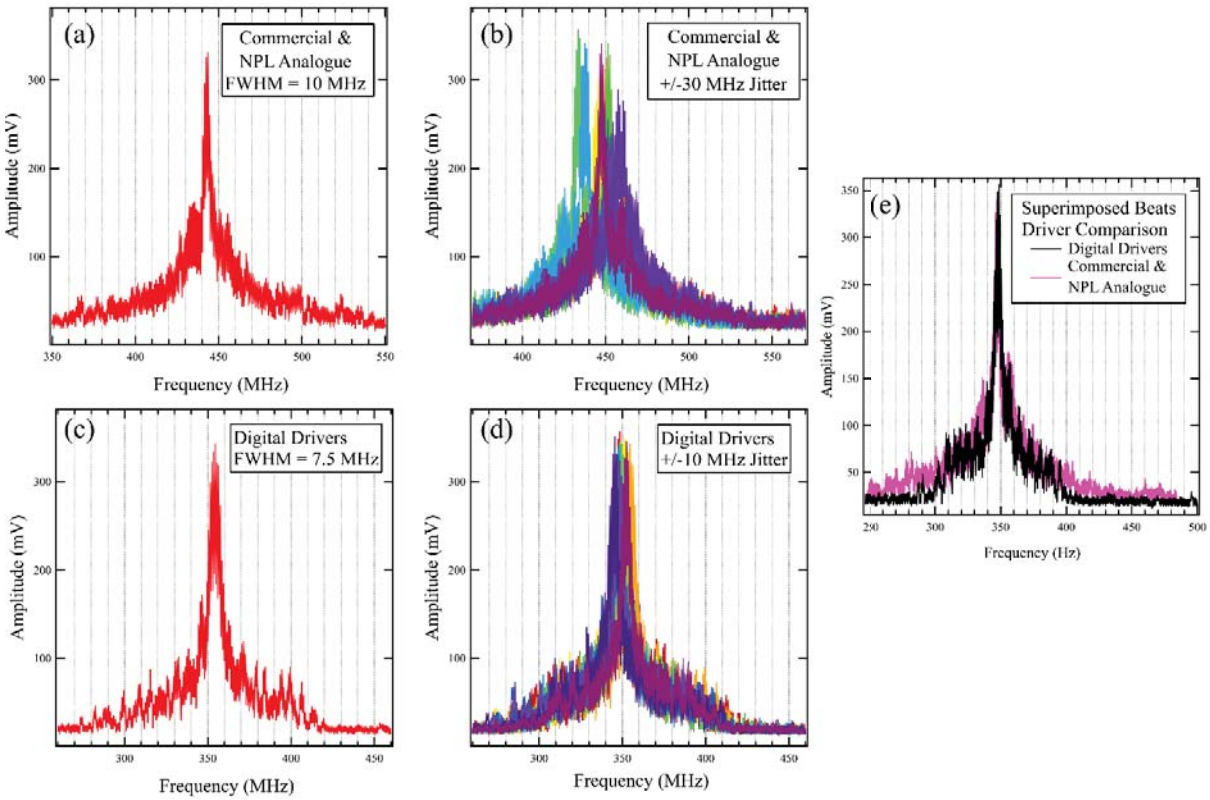

Figure 5.8 Resultant beats from Eblana 1854 nm DFB lasers. The (a) linewidth and (b) jitter from beats obtained using a commercial driver and an NPL analogue driver. The (c) linewidth and (d) jitter using the low noise digital drivers shows improvement. (e) A representative beat from each current driver configuration superimposed highlights the reduction in noise.

Figure 5.8 compares the beats produced between two Eblana 1854 nm diode lasers using (a,b) a commercial and NPL analogue current driver combination and (c,d) digital current drivers. The

representative FWHM is 10 MHz using the commercial-NPL analogue current driver configuration is reduced to 7.5 MHz when driven using the digital drivers. Moreover the frequency jitter is markedly improved from 30 MHz to 10 MHz as shown in 5.8 b and d. Figure 5.8e superimposes (a) and (c) to better show the reduction in noise, particularly with respect the lineshape wings which is likely due to flicker noise [14].

Table 5.1 Overview comparison of beat characteristics.

Driver Type	1742 nm		1854 nm	
	HWHM (MHz)	Jitter (MHz)	HWHM (MHz)	Jitter (MHz)
Commercial & NPL Analogue	5	>55	5	30
Digital	5	50	2.5	10

Table 5.1 compares the resultant 1742 nm and 1854 nm beat parameters obtained from figure 5.7 and figure 5.8. Since the two lasers are manufactured in the same batch, it is assumed that the laser output is approximately identical. Therefore, the laser linewidth of each laser is assumed to be the half width at half maximum of the beat linewidth. Interestingly, there is marked improvement with the output characteristics of the 1854 nm pair compared to the 1742 nm pair. However, in both beat measurements the overall signal noise is clearly reduced.

5.4 Experimental setup

An overview of the key experimental requirements for the dual HCl/H_2O NICE-OHMS system is shown in figure 5.9. DFB lasers at 1742 nm and 1854 nm, for HCl and H_2O spectroscopy respectively, are aligned into the same cavity. The system is designed such that only one frequency is locked to the cavity at a time. Ideally the water content in the cavity is assessed using the 1854 nm laser immediately before HCl measurements which use the 1742 nm laser. Both lasers share the same locking electronics which is represented by the dashed arrows in figure 5.9. The carrier frequency, f_c, is locked to the cavity FSR by adding 15 MHz (δ) sidebands for a PDH locking scheme [15, 16] . Since only frequencies at the FSR of the cavity can be enhanced/sustained inside the cavity, the NICE-OHMS sidebands added for the cavity enhanced frequency modulation need to be at the FSR which is ~1.5 GHz. Using a DeVoe-Brewer locking scheme [4], the NICE-OHMS sidebands are also locked to the FSR of the cavity by mixing the same 15 MHz signal used for PDH locking with the ~1.5 GHz signals together and using the FSR-δ frequency as a reference signal for DBM 3.

In short, use of the same 15 MHz signal for both the PDH and DVB locking schemes is essential in ensuring both the carrier frequency and FSR sidebands are always frequency stabilised/locked to the cavity. To optimise the down mixed frequencies signals generated by the DBMs, pass band filters are used to ensure only the relevant frequencies detected by the light reflected by the cavity are used in each scheme. Similarly, phase shifters are added to one of the mixer inputs to maximise the down mixed signal.

Gas is flowed into the cavity at a low flow rate (~0.8 L/min) to enable gas diffusion through the system at atmospheric pressure. The inlet and outlet gas ports are positioned near each cavity mirror to ensure gas entering and leaving the chamber interacts with the optical cavity path. To sweep the frequency modulated light through either the H_2O or HCl feature, the laser frequency is locked to the TEM_{00} mode of the cavity and is adjusted by changing the cavity length using a piezoelectric (PZT) tube which one of the mirrors is mounted on. Explicitly, the DVB locking scheme adjusts the frequency of the NICE-OHMS

sidebands to match the FSR as the cavity length is adjusted. The output NICE-OHMS signal is given according to equation (1) where the DC output of the down mixed signal is proportional to the absorption through the gas.

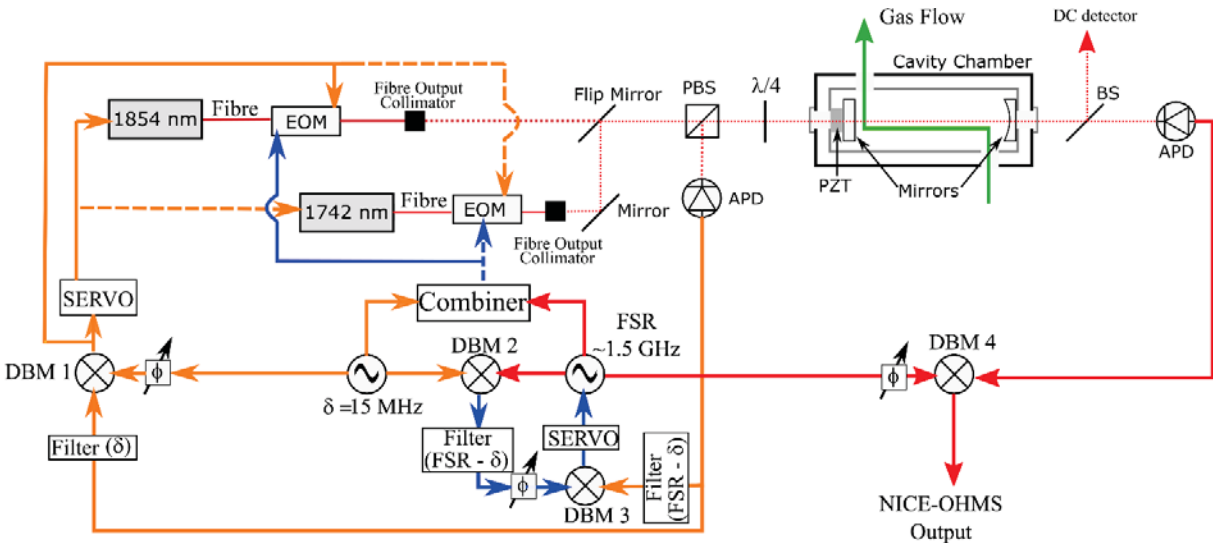

Figure 5.9 Schematic of experimental layout for NICE-OHMS. Dashed red line corresponds to free space laser light. The orange solid line corresponds to 15 MHz signal and RF signals needed for Pound-Drever-Hall locking scheme (dashed orange line represent that the same electronics is shared between the two lasers). The red solid lines correspond to the ~1.5 GHz/FSR signal used for the NICE-OHMS signals. The blue solid lines correspond the DVB scheme to lock the sidebands at ~1.5 GHz to the cavity free spectral range. The filters show what frequencies pass in brackets. Variable phase shifters are used to phase match both signals that enter the DBMs to optimise performance.

5.5 Gas sampling system

5.5.1 Materials of choice

The materials used in the gas sampling system are specific to the selected AMC; for example, in the NICE-OHMS system developed for ammonia [7] copper was avoided (e.g. as a material for gasket seals). This is because copper is reported to react strongly with ammonia, particularly in the presence of trace moisture levels. Our cavity spacer is made from Super Invar and we showed [7] that this had a negligible influence on ammonia surface adsorption. Also, the flow geometry of our system did not introduce significant dead volumes, which might slow down the time to reach steady state. For HCl, we will use a similar cavity geometry as to that demonstrated for ammonia, except all stainless steel and Super Invar surfaces will be treated with a Silkonert2000® passivation coating [17]. HCl and water are sticky gases and upon interaction with an uncoated surface are likely to adsorb to the surface with a low/negligible desorption rate. This decreases the concentration of HCl/H_2O in the measurement region and will give an inaccurate result. Part 2 of deliverable report D1 discusses this in detail. Passivation coatings provide a surface with a lower sticking probability than stainless steel and Super invar such that typically “sticky” molecules like HCl and H_2O are less likely to be removed from the measurement system due to surface adsorption interactions. Therefore, this coating significantly decreases the conditioning time required prior to trace gas measurements.

5.5.2 Sampling system

For HCl, we plan to use a similar arrangement to that described in [7] for ammonia with a typical flow rate of 0.8 l/min through the cavity spacer. The different trace concentrations will be provided via a high-accuracy, self-referencing dilution device that consists of a binary network of critical flow orifices [18]. During all measurements, dry nitrogen is used to carry the pre-determined trace HCl gas through the NICE-OHMS system. However, prior to any HCl measurement campaign, the NICE-OHMS system will be flushed with dry nitrogen to remove any water impurities. During the nitrogen purge, the system will spectroscopically assess the water content in the chamber using the 1854 nm laser.

5.6 Recommendations to instrument operation

5.6.1 Calibration

A procedure for the calibration of a NICE-OHMS spectrometer will be drafted after the end of the project and will incorporate the input from both this work and the first MetAMC project. As part of future activity to determine the calibration procedure, we will also draft an operational procedure for the NICE-OHMS device.

5.7 Standard tests and results

The parameters to be determined for any AMC spectroscopic measurement device were described in Reference [19] and are listed below, together with a brief description of the terminology. A fuller description in each case is given in a report on the project website, in our recommendations for lab and field testing[1].

- Working range: This describes the measurement capability of the device in terms of concentrations of HCl it can accurately measure
- Limit of detection (LOD): This is defined as $3\sigma/S$, where σ is the standard deviation of the noise of the instrument and S the instrument sensitivity.
- Measurement uncertainty: This should be estimated for all concentrations in the “working range”
- Instrument response and recovery time: How long it takes the measurement system to come to the equilibrium measurement value (decided by the partners, e.g. time to 90% full value)
- Effects of other gas species on measurement: Depending on how the device acquires and analyses data, there is a concern that measurements of HCl may be affected by the presence of other gas species.
- Zero drift measurement: The measurement stability of the baseline of the device when flowing air through the system.
- Span drift measurement: The stability of the measurement of a fixed HCl concentration over different time scales
- Effects on measurement when changing temperature and/or humidity and/or pressure and/or flow rate through the analyser

[1] http://empir.npl.co.uk/metamcii/impact-output/

5.8 Conclusions

At NPL we are developing a NICE-OHMS-based device for detection of HCl in an industrial environment. For ultra-sensitive detection at 1 ppb and below we have chosen to detect on a transition at 1742 nm to facilitate the use of commercially available and fibre coupled lasers (with integrated isolators), modulators, and mirror coatings the production of ultra-high finesse cavities (which can also be used for water vapour detection at 1854 nm.) We have modelled the expected NICE-OHMS signal for our device for HCl concentrations in the region between 1 ppb and 1 ppm, which requires extended theories for correct results. Initial tests of current drivers show that commercial devices add unwanted noise to the laser linewidth, and we will be proceeding with in-house digital current controller designs. We have investigated passivation coatings for the gas lines and for the NICE-OHMS cavity cell and will be using a Silkonert2000® to help mitigate the potentially deleterious effect of HCl on our system, even at such low concentrations. Finally, we have produced a protocol for measurement and calibration of the NICE-OHMS system, which will be more fully explored and implemented in the testing stage of the project.

5.9 References

[1] J. L. Hall, L. Hollberg, T. Baer and H. G. Robinson, "Optical heterodyne saturation spectroscopy," Appl. Phys. Lett., vol. 39, pp. 680-2, 1981.

[2] J. Wang, P. Ehlers, I. Silander and O. Axner, "On the accuracy of the assessment of molecular concentration and spectroscopic parameters by frequency modulation spectrometry and NICE-OHMS," Journal of Quantitative Spectroscopy & Radiative Transfer, vol. 136, pp. 28-44, 2014.

[3] J. Ye, L.-S. Ma and J. L. Hall, "Ultrasensitive detections in atomic and molecular physics: demonstration in molecular overtone spectroscopy," J. Opt. Soc. Am. B, vol. 15, pp. 6-15, 1999.

[4] R. G. DeVoe and R. G. Brewer, "Laser-frequency division and stabilization," Phys Rev A, vol. 30, p. 2827–2829, 1984.

[5] W. Ma, I. Silander, T. Hausmaninger and O. Axner, "Doppler-broadened NICE-OHMS beyond the cavity-limited weak absorption condition – I. Theoretical description," Journal ofQuantitative Spectroscopy & Radiative Transfer, vol. 168, pp. 217-244, 2016.

[6] T. Hausmaninger, I. Silanderr, W. Ma and O. Axner, "Doppler-broadened NICE-OHMS beyond the cavity-limited weak absorption condition – II: Experimental verification," Journal of Quantitative Spectroscopy & Radiative Transfer, vol. 168, pp. 245-256, 2016.

[7] E. A. Curtis, G. P. Barwood, G. Huang, C. S. Edwards, B. Gieseking and P. J. Brewer, "Ultra-high-finesse NICE-OHMS spectroscopy at 1532 nm for calibrated online ammonia detection," JOSA B, vol. 34, pp. 950-8, 2017.

[8] D. Z. Anderson, "Alignment of resonant optical cavities," Applied Optics, vol. 23, no. 17, pp. 2944-2949, 1984.

[9] H. Kogelnik and T. Li, "Laser Beams and Resonators," Applied Optics, vol. 5, no. 10, pp. 1550-1567, 1966.

[10] N. Barre, M. Romanelli, M. Lebental and M. Brunel, "Waves and rays in plano-concave laser cavities: I. Geometric modes in the paraxial approximation," European Journal of Physics, vol. 38, no. 3, p. 034010, 2017.

[11] G. Shen, X. Chao and K. Sun, "Modeling the optical field in off-axis integrated-cavity-output spectroscopy using the decentered Gaussian beam model," Applied Optics, vol. 57, no. 11, pp. 2947-2954, 2018.

[12] K. G. Libbrecht and J. L. Hall, "A low-noise high-speed diode laser current controler," Review of Scientific Instruments, vol. 64, no. 8, pp. 2133-2135, 1993.

[13] C. J. Erickson, M. Van Zijll, G. Doermann and D. S. Durfee, "An ultrahigh stability, low-noise laser current driver with digital controls," Review of scientific instruments, vol. 79, no. 7, p. 073107, 2008.

[14] G. Di Domenico, S. Schilt and P. Thomann, "Simpe Approach to the relation between laser frequency noise and laser line shape," Applied Optics, vol. 49, no. 25, pp. 4801-4807, 2010.

[15] R. Drever, J. L. Hall, F. V. Kowalski, J. Hough, G. M. Ford, A. J. Munley and H. Ward, "Laser phase and frequency stabilization using an optical resonator," Applied Physics, vol. 31, no. 2, pp. 97-105, 1983.

[16] E. D. Black, “An introduction to Pound--Drever--Hall laser frequency stabilization,” American journal of physics, vol. 69, no. 1, pp. 79-87, 2001.
[17] P. Harris and M. Pelligrinni, “Mass Transport in Sample Transport lines Adsorption Desorption Effects and their Influence on Process Analytical Measurements,” in International Society of Automation 56th Analysis Division Symposium, 2011.
[18] P. J. Brewer, B. A. Goody, T. Gillam, R. C. J. Brown and M. J. T. Milton, “High-accuracy stable gas flow dilution using an internally calibrated network of critical flow orifices,” Measurement Science & Technology, vol. 21, p. 115902, 2010.
[19] Analytical Methods Committee, “Recommendations for the definition, estimation and use of the detection limit,” Analyst 112, 199-204, 1987.
[20] H. Kogelnik and T. Li, “Laser beams and resonators,” Applied Optics, pp. 1550-67, 1966.
[21] R. a. B. R. DeVoe, “Laser-frequency division and stabilization,” Physical Review A, vol. 30, no. 5, p. 2827, 1984.

III. Summary

This report encompasses a summary on the potential and capabilities of the state-of-the-art high-resolution spectrometers developed to detect challenging gaseous species such as HCl at lower than one parts-per-billion by volume (ppbv), with response times under one minute. The design aspects of the different spectrometers have been described. The advantages and disadvantages of various techniques are also presented. The high accuracy static and dynamic HCl reference materials developed in WP2 will be used for calibration of the various spectrometers and periodic validation. There are currently no standards realised for HCl at low amount fractions (< 100 ppm). The measurements using the various spectrometers on the dynamic and static reference materials developed in WP2 in an intercomparison campaign within the various NMIs will help underpin HCl amount fractions at the parts-per-billion range which are important in applications such as AMC monitoring in semiconductor fabs. The spectrometers developed (expect the PTB-OGS and VSL CRDS-OPO) will be employed for field testing campaigns in cleanroom manufacturing facilities.